Article

Cell Reports

Heat-Shock Protein 90 Controls the Expression of Cell-Cycle Genes by Stabilizing Metazoan-Specific Host-Cell Factor HCFC1

Graphical Abstract

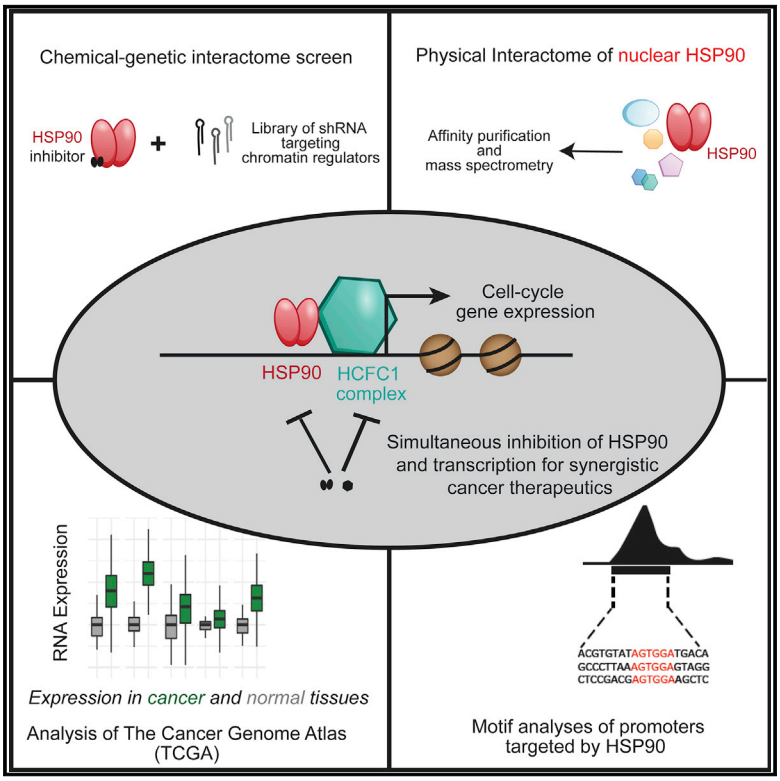

Highlights

- Comprehensive genetic and physical interactome of nuclear HSP90 in human cells
- HSP90 stabilizes HCFC1 complex at chromatin to drive cell-cycle gene expression
- Synergistic killing of cancer cells by simultaneous inhibition of HSP90 and HCFC1

Authors

Aneliya Antonova, Barbara Hummel, Ashkan Khavaran, ..., Gerhard Mittler, Cornelius Miething, Ritwick Sawarkar

Correspondence

rs2099@cam.ac.uk

In Brief

What do chaperones do in the nucleus? Antonova et al. perform a comprehensive genetic and physical interactome analysis of nuclear HSP90 in human cells. HSP90 stabilizes the HCFC1 complex at chromatin, contributing to the expression of HCFC1-targeted cell-cycle genes. The simultaneous inhibition of HSP90 and transcription is synergistic in killing cancer cells.

Antonova et al., 2019, Cell Reports *29*, 1645–1659
November 5, 2019
https://doi.org/10.1016/j.celrep.2019.09.084

CellPress

Cell Reports
Article

Heat-Shock Protein 90 Controls the Expression of Cell-Cycle Genes by Stabilizing Metazoan-Specific Host-Cell Factor HCFC1

Aneliya Antonova,[1,4,9] Barbara Hummel,[1,9] Ashkan Khavaran,[1,5] Desiree M. Redhaber,[2,3,4] Fernando Aprile-Garcia,[1] Prashant Rawat,[1,4] Kathrin Gundel,[1] Megan Schneck,[1] Erik C. Hansen,[1] Jan Mitschke,[3] Gerhard Mittler,[1] Cornelius Miething,[2,3,6] and Ritwick Sawarkar[1,7,8,10,*]

[1]Max Planck Institute of Immunobiology and Epigenetics, Freiburg, Germany
[2]German Consortium for Translational Cancer Research (DKTK), Partner Site Freiburg and German Cancer Research Center (DKFZ), Heidelberg, Germany
[3]Department of Hematology, Oncology and Stem Cell Transplantation, Faculty of Medicine, Medical Center - University of Freiburg, Freiburg, Germany
[4]Faculty of Biology, University of Freiburg, Freiburg, Germany
[5]Faculty of Medicine, University of Freiburg, Freiburg, Germany
[6]BIOSS Centre for Biological Signalling Studies, University of Freiburg, Freiburg, Germany
[7]CIBSS Centre for Integrative Biological Signalling Studies, University of Freiburg, Freiburg, Germany
[8]MRC Toxicology Unit, University of Cambridge, Cambridge, UK
[9]These authors contributed equally
[10]Lead Contact
*Correspondence: rs2099@cam.ac.uk
https://doi.org/10.1016/j.celrep.2019.09.084

SUMMARY

Molecular chaperones such as heat-shock proteins (HSPs) help in protein folding. Their function in the cytosol has been well studied. Notably, chaperones are also present in the nucleus, a compartment where proteins enter after completing *de novo* folding in the cytosol, and this raises an important question about chaperone function in the nucleus. We performed a systematic analysis of the nuclear pool of heat-shock protein 90. Three orthogonal and independent analyses led us to the core functional interactome of HSP90. Computational and biochemical analyses identify host cell factor C1 (HCFC1) as a transcriptional regulator that depends on HSP90 for its stability. HSP90 was required to maintain the expression of HCFC1-targeted cell-cycle genes. The regulatory nexus between HSP90 and the HCFC1 module identified in this study sheds light on the relevance of chaperones in the transcription of cell-cycle genes. Our study also suggests a therapeutic avenue of combining chaperone and transcription inhibitors for cancer treatment.

INTRODUCTION

Molecular chaperones stabilize or help proteins acquire a native conformation, but are themselves not present in the final functional structure (Hartl, 1996). In conjunction with the protein degradation machinery, molecular chaperones influence the half-lives of proteins controlling protein homeostasis or proteostasis. Initially defined as heat-shock proteins (HSPs) owing to their stress responsiveness (Richter et al., 2010), chaperones are classified based on their structure and function in various families such as HSP70 and HSP90. While HSP70 is required for early events in polypeptide folding, HSP90 interacts with a limited set of proteins, called clients, that are almost fully folded. There is no common sequence, structure, or function among the diverse HSP90 clients. Rather, exposure of hydrophobic residues over a long stretch and general conformational instability appears to define HSP90 clients (Taipale et al., 2012). Metastable proteins such as steroid receptors and signaling kinases exemplify HSP90 clients. The N-terminal ATPase domain of HSP90 powers the chaperoning process, while the C-terminal domain is required for homodimerization. A suite of co-chaperones, including p23, AHA1, and CDC37, drive the conformation cycle of the chaperone and/or deliver clients to HSP90 (Li et al., 2012). The HSP90 chaperone system also helps in the assembly and disassembly of protein complexes with the help of specific co-chaperones (Freeman and Yamamoto, 2002; Makhnevych and Houry, 2012).

The unique role of HSP90 in the folding landscape of the cellular proteome coupled with its high levels in unstressed cells confer upon HSP90 unexpected functions in evolution and cancer (Rutherford and Lindquist, 1998). Even if HSP90 levels are high in normal cells, they further increase in several cancers (Hadizadeh Esfahani et al., 2018; Pick et al., 2007; Whitesell and Lindquist, 2005). Cancer cells were found to be more sensitive than normal cells to small-molecule inhibitors of the ATPase activity of HSP90, prompting several clinical trials in cancer patients (Canonici et al., 2018; Trepel et al., 2010). HSP90 facilitates and/or maintains neoplastic transformation, causing an increased dependence of cancers on the HSP90 chaperone system. The precise mechanism by which HSP90 supports tumor

proliferation remains ill-defined, but likely involves chaperoning a number of oncogenic drivers (Vartholomaiou et al., 2016). A recent study argued that the active maintenance of the cell cycle in cancer cells makes them more sensitive to an HSP90 inhibitor (hereafter referred to as HSP90in) (Echeverria et al., 2019). Thus, HSP90 represents a key chaperone system that is conserved from bacteria to human, essential for viability in eukaryotes and relevant for evolution and cancer. An understanding of the breadth of HSP90 function in the cellular context requires exhaustive definition of its clients and co-chaperones. Systems-wide studies in yeast have outlined the genetic and physical interactome of HSP90 (McClellan et al., 2007; Millson et al., 2005; Zhao et al., 2005), illuminating the different cellular processes HSP90 contributes to. Similar global studies in metazoan are technically challenging and have recently been reported, widening our understanding of HSP90 functions (Echeverría et al., 2011; Falsone et al., 2005, 2007; Gano and Simon, 2010; Moulick et al., 2011a; Taipale et al., 2012, 2014; Tsaytler et al., 2009).

Human HSP90 is encoded by two paralogs, HSP90α and HSP90β, in addition to endoplasmic reticulum (ER)-specific GRP94 and mitochondria-specific TRAP1. Early studies indicated that ~2%–3% of the cellular pool of HSP90 resides in the nucleus (Berbers et al., 1988; Perdew et al., 1993). Unlike the ER and the mitochondria, the nucleus imports proteins that have completed *de novo* folding in the cytosol. Thus, the nucleus presents a unique opportunity to study the function of chaperones in steps of proteostasis, such as protein stabilization and complex assembly, after completion of the initial folding of proteins. We and others have shown that HSP90 binds chromatin and influences gene expression (Cvoro et al., 2006; Freeman and Yamamoto, 2002; Greer et al., 2015; Moulick et al., 2011a; Sawarkar et al., 2012). The molecular mechanism by which HSP90 regulates transcription at the sites of gene expression is not fully known. By directly interacting with chromatin-associated proteins, HSP90 may help nucleosome disassembly and regulate the transcriptional pausing/elongation checkpoint (Gvozdenov et al., 2019; Sawarkar et al., 2012). HSP90 and p23 control the residence time of proteins bound to chromatin by evicting protein complexes from chromatin (Echtenkamp et al., 2016). High nuclear HSP90 has been shown to correlate with poor prognosis in a long-term study of a cohort of patients with non-small-cell lung cancer (NSCLC) (Su et al., 2016). Given that many cancers are driven by transcriptional regulators, it is highly likely that cancer-promoting transcription programs are stabilized by the chaperone activity of HSP90 in the nucleus (Calderwood and Neckers, 2016; Isaacs, 2016). Moreover, both transcription and HSP90 have been independently targeted in cancer therapeutics. Understanding mechanisms by which HSP90 regulates transcription may pave the way for a rational synergistic combination of cancer therapeutics targeting the chaperone and transcription. Hence, the complete realm of HSP90 activity in the nucleus must be thoroughly investigated. For this purpose, we need to define the spectrum of clients and co-chaperones of nuclear HSP90 in mammalian cells. Published interaction studies in the context of human cells have been performed primarily in cytosol or total cell extract (Falsone et al., 2005, 2007; Gano and Simon, 2010; Moulick et al., 2011; Sharma et al., 2012; Taipale et al., 2014; Tsaytler et al., 2009), wherein nuclear interactions are either lost or outnumbered by the large amount of cytosolic HSP90 pool. While physical interactomes of chaperones generate lists of several hundred proteins, genetic interactions can be used to prioritize clients that are functionally important. Given the importance of HSP90 in cancers, harnessing the gene expression data available for numerous tumor samples would allow us to further narrow down the nuclear HSP90 interactors with potential relevance to oncogenesis.

RESULTS

In this study, we systematically analyzed the functional interactions of nuclear HSP90 in human cells by using three orthogonal and independent approaches: (1) a chemical-genetic screen to quantitate the genetic interactions of HSP90 with transcriptional regulators, (2) affinity purification of nuclear HSP90 to identify direct physical interactors in the nucleus, and (3) a computational analysis to identify transcriptional regulators that are co-expressed with HSP90 in cancer patient datasets. The individual approaches are described below.

A Screen to Identify Chromatin Regulators Functionally Interacting with HSP90

The proliferation of cancer cells is sensitive to HSP90 inhibition using small molecules that target the ATPase activity of the chaperone (Tao et al., 2015; Wang et al., 2013a). HSP90 is likely required for the stabilization of a subset of proteins that is critical for cell proliferation. The partial depletion of such proteins by knock down is expected to make cancer cells even more sensitive to sublethal concentrations of HSP90 inhibitors. Based on this idea, we performed a chemical-genetic screen to identify genes that when knocked down enhance/reduce the sensitivity of cells to the HSP90in. For HSP90in, we used NVP-AUY922, a drug that is in phase II clinical trials against several cancers (Brough et al., 2008; Eccles et al., 2008). This drug is expected to inhibit both cytosolic and nuclear pools of HSP90. We used human erythroleukemic cell line K562 as a cellular model to address the functional contribution of HSP90 to oncogenic proliferation. We leveraged the approach of barcoded small hairpin RNA (shRNA) pooling (Scuoppo et al., 2012), in which pools of shRNAs targeting hundreds of genes are used to transduce a cell population (Figure 1A). The proportion of cells carrying each shRNA in a mixed population is quantified by deep sequencing of barcodes. Thus, the difference in shRNA frequency in populations exposed to vehicle compared to HSP90in will represent the quantitative effect of HSP90 inhibition on the proliferation of cells expressing an individual shRNA. This allowed us to infer the chemical-genetic interaction score (CGIS) of the target gene. A negative CGIS of a gene indicates that cells depleted of the corresponding protein were more sensitive to HSP90in than control cells. To focus on the function of nuclear HSP90 in gene expression, we used a library of pooled shRNA targeting 677 genes with the Kyoto Encyclopedia of Genes and Genomes (KEGG) pathway annotation as chromatin/transcriptional regulation (Table S1). Each of the 677 genes was targeted using 4 independent

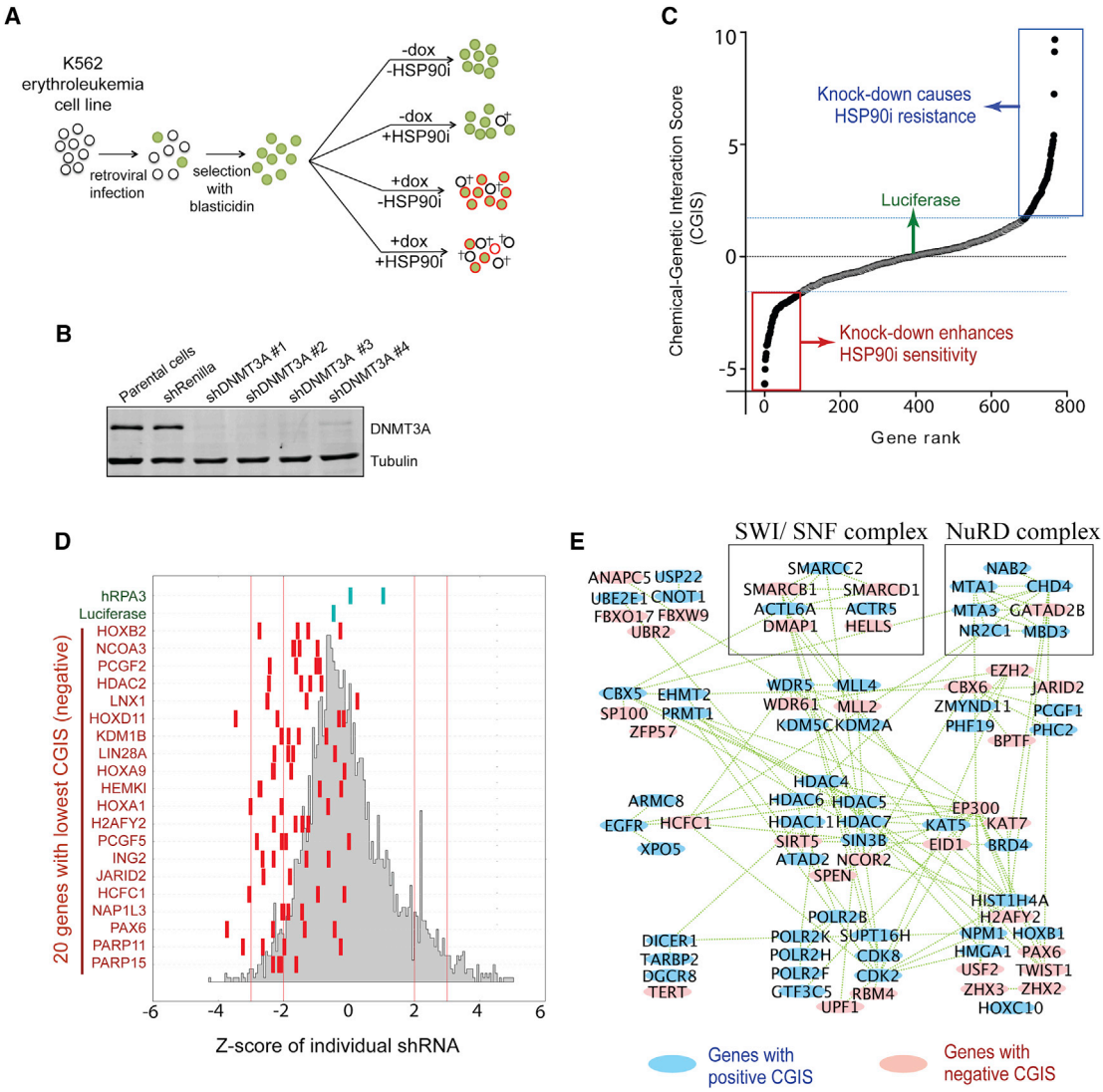

Figure 1. Chemical-Genetic Screen for HSP90 Interactors

(A) Outline of the experimental approach. The K562 erythroleukemia cell line (black circles) was retrovirally infected to introduce the barcoded shRNA library and selected for blasticidin-resistant cells (green circles). shRNA expression was induced (red circles) by the addition of doxycycline (dox). HSP90 inhibitor (NVP-AUY922) was added as shown. Black circles with a dagger sign indicate dead cells. Four days after dox and/or HSP90 inhibitor treatment, cells were harvested from each pool and barcode frequency was determined by deep sequencing to calculate the chemical-genetic interaction score (CGIS; see Method Details).

(B) Representative western blot analysis of DNMT3A expression in K562 cells, showing the effect of individual shRNAs targeting DNMT3A or Renilla. Tubulin is used for normalization.

(C) Waterfall plot showing CGIS of all 668 genes screened in the experiment on the y axis plotted against the gene rank from lowest to highest CGIS. Thresholds used to shortlist HSP90 interactors are indicated with horizontal blue lines.

(D) *Z* scores of individual shRNAs (red boxes) targeting 20 genes with the lowest CGISs identified in the screen are shown. The gray histogram depicts the normalized distribution of *Z* scores of all of the candidates in the screen. Control shRNAs (see Method Details) are highlighted as blue boxes. Red vertical lines indicate the 66th and the 98th percentile in *Z* scores on either side of zero.

(E) A subset of genes identified with significant positive (blue) or negative (pink) CGIS from (C) are shown in a network derived using Cytoscape. Genes encoding the components of a complex or proteins in the same functional pathway are shown together. Lines connecting individual genes indicate interactions known in the literature. The two boxes indicate complexes of which multiple subunits and related proteins were identified in the screen.

See also Figures S1 and S2 and Tables S1 and S2.

shRNAs (Figure 1B) to reduce the influence of off-target effects on CGIS. Furthermore, we used the doxycycline-inducible shRNA library (Figure S1) to minimize the long-term consequences of knocking down critical genes.

We performed the chemical-genetic screen using HSP90in on K562 cells in two replicates that showed high reproducibility (Figure S2A). The shRNA targeting luciferase had a CGIS of ~0 (Figures 1C, 1D, and S2B), as expected for the negative control. The

average SD for all shRNAs targeting the same gene was ~0.07, indicating highly reproducible effects between the different shRNAs (Figure 1D). Thus, our chemical genetic screen yielded robust CGISs for all 677 tested genes. With a cutoff of |CGIS| > 1.5, we identified 203 genes that genetically interact with human HSP90 in the context of K562 cells: 103 genes with positive CGISs and 100 with negative CGISs (Table S2). Proteins known to interact with HSP90 in yeast and flies, such as the Polycomb/trithorax group and the switch/sucrose non-fermentable (SWI/SNF), were recovered in the chemical-genetic screen in human K562 cells validating our approach (Figures 1D and 1E; Table S2; Hummel et al., 2017; McClellan et al., 2007; Millson et al., 2005; Tariq et al., 2009; Zhao et al., 2005). The chi-square test showed a non-significant overlap between genetic interactors identified here and known clients of HSP90 (https://www.picard.ch/HSP90Int/index.php). This is likely due to the fact that known clients are mostly cytosolic, underestimating transcription regulators on which our screen focused (Figure 1). Thus, the chemical-genetic interaction screen identified several chromatin regulators that had not been known to interact with HSP90.

Physical Interaction Network of Nuclear HSP90 in Human Cells

Genetic interactions can be attributed to an indirect relation between the two interacting genes. In the context of HSP90, the candidates we identified in the chemical-genetic interaction screen need not be clients of the chaperone. Knocking down such genes may rescue the detrimental effects of HSP90 inhibition on proliferation or affect proteostasis, making cells more dependent on unrelated processes that are contingent on HSP90 (Li et al., 2015). The physical protein-protein interactome can provide a complementary approach by confirming direct contact between genetically interacting proteins. Only 2%–3% of total cellular HSP90 is in the nucleus (Berbers et al., 1988; Perdew et al., 1993), and hence, previous attempts to find HSP90 interactors in total cell extracts have yielded mostly cytosolic proteins (Falsone et al., 2005, 2007; Gano and Simon, 2010; Taipale et al., 2014; Tsaytler et al., 2009). We sought to identify proteins that physically interact with nuclear HSP90 by affinity purification coupled to mass spectrometry (AP-MS) after the subcellular fractionation of human cells (Figure 2A). Given that HSP90α binds some clients with higher affinity than HSP90β (Prince et al., 2015b), we focused on the former for AP-MS. We used HEK293 Flp-In T-Rex cells (Hauri et al., 2016) expressing HSP90α N-terminally tagged to Strep-tag to identify the interactors of nuclear HSP90. The HEK293 system has been extensively used for interactome analyses of several key cellular proteins, allowing us to contribute to a widely usable resource and linking our data with pre-existing information (Hauri et al., 2016). Tetracycline-inducible production ensured levels of tagged HSP90 lower than the endogenous protein (Figure 2B). We used nuclear extracts of induced cells to perform StrepTactin-based AP-MS in four independent biological replicates. Cells expressing red fluorescent protein (RFP) instead of HSP90α acted as a negative control. The proteins identified in HSP90α and RFP AP-MS were statistically analyzed to identify the interactors of nuclear HSP90α (Figure S3A; Table S3). The analysis focused on intensity ratios of peptides identified in RFP versus HSP90 samples, as well as reproducibility across replicates, as has been done before (Cox et al., 2014; Mosley et al., 2011; ten Have et al., 2011) and as detailed in Method Details. Since cytosolic HSP90 is much more abundant than the nuclear counterpart, we made sure that cytosol did not contaminate the nuclear extracts used to identify the HSP90 interactome. First, the purity of nuclear extracts was confirmed using western blotting before AP-MS (Figure 2C). Second, Gene Ontology analysis of proteins identified in AP-MS confirmed that mostly nuclear proteins were enriched, ruling out cytosolic contamination (Figure S3B). Third, kinases present in the cytoplasm known to be HSP90 clients, such as B-RAF and c-SRC, were not identified in our AP-MS (Table S3). Instead, 9 of 10 kinases that we identified were known to have nuclear functions (Table S3).

The resulting complex network of HSP90 binding partners comprised proteins falling into the following main categories: (1) chaperones and co-chaperones, (2) components of the protein degradation machinery, (3) DNA repair proteins, (4) RNA metabolism factors, and (5) transcription regulators. We recovered several proteins known to interact with HSP90, such as RNA polymerase II (Pol II) pausing/elongation proteins (Figures 2D and 2E; Table S3; Hummel et al., 2017; Sawarkar et al., 2012; Sharma et al., 2012). From ~450 proteins (Table S3), we focused on transcription regulators only, and we manually curated 102 proteins as high-confidence interactors of nuclear HSP90 with roles in transcription (Figure 2E; Table S4). Of these, only six were previously reported to be HSP90 interactors (https://www.picard.ch/HSP90Int/index.php). The large number of hitherto unidentified interactions seen in our analysis (Table S4) may stem from the fact that the low-abundance transcriptional regulators are diluted in total cell extracts that had thus far been used in the field. It should be noted that the nuclear interactome and the chemical-genetic screen were performed in two different cell lines. A direct correlation between the output of these two screens may not be appropriate without any further biochemical validation.

Genes Co-expressing with HSP90 in Cancer Tissues

The genetic and physical interactions of HSP90 presented in this study thus far have been carried out in cell lines cultured in the lab that may be very different from the actual cancer cells from patients. We argued that if the expression of cancer-relevant interactors of HSP90 is higher in cancer cells compared to normal cells, then the expression of HSP90 may also be higher in cancer cells that are likely to stabilize those interactors. We tested this idea using transcriptional regulators that associate with nuclear HSP90 (Figure 2E; Table S4). We harnessed publicly available cancer RNA expression data from The Cancer Genome Atlas (TCGA; https://www.cancer.gov/about-nci/organization/ccg/research/structural-genomics/tcga), as large-scale quantitative data on protein abundance in cancer cells are not available. We focused on datasets from 17 cancers encompassing 7,080 patients and 710 healthy controls in total. We confirmed that HSP90 is transcriptionally upregulated in 12 of 17 types of cancers compared to the corresponding healthy tissues (Figure 3A), as has been shown before (Hadizadeh Esfahani et al., 2018; Whitesell and Lindquist, 2005). The physical interactors

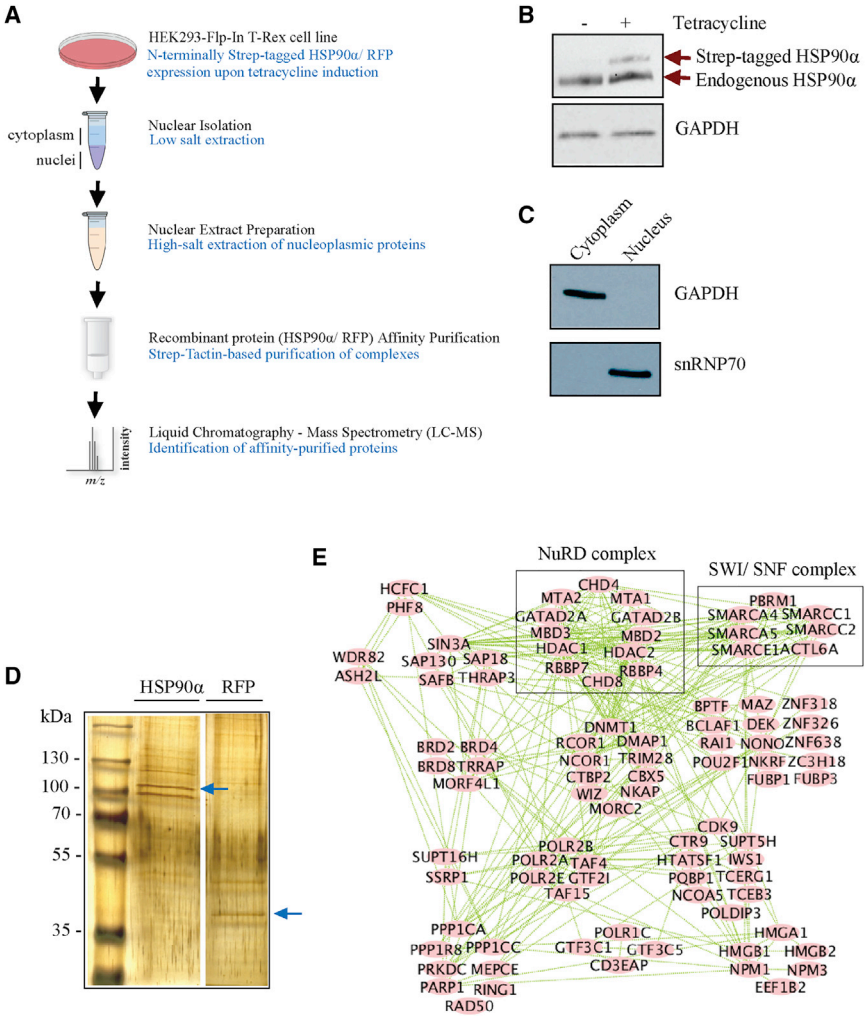

Figure 2. Physical Interactome of Nuclear HSP90α in Human Cells

(A) Schematic overview of the experimental protocol.

(B) Expression of recombinant HSP90α upon tetracycline induction in the HEK293 cell line demonstrated by western blot of cell extracts. Glyceraldehyde 3-phosphate dehydrogenase (GAPDH) is used for normalization.

(C) Purity of cellular fractions as demonstrated by western blot using small nuclear ribonucleoprotein particle 70 (snRNP70) as a nuclear marker and GAPDH as a cytosolic marker.

(D) Visualization of affinity-purified HSP90-bound complexes by SDS-PAGE and silver staining. RFP-expressing HEK293 cells were used as a negative control. The blue arrows indicate the expected position of the tagged proteins. The lanes between HSP90α and RFP from the original gel picture were removed for clarity.

(E) Transcription regulators identified as physical interactors of HSP90α are shown in a network derived using Cytoscape. Genes encoding the components of a complex or proteins in the same functional pathway are shown together. Lines connecting individual genes indicate interactions known in the literature. The two boxes indicate complexes of which multiple subunits and related proteins were identified in the interactome.

See also Figure S3 and Tables S3 and S4.

of nuclear HSP90 identified in this study (Figure 2E; Table S4) are significantly upregulated in most of the cancer types in which HSP90 levels are higher (Figure S4A). The inference holds true even after increasing the stringency of the cutoff for identifying interactors (Figure S4B). This observation motivated us to perform an unbiased search for transcription regulators whose expression correlates with the expression of HSP90 across all 17 cancer types. We constructed an expression-correlation matrix using data from individual cancer patients or healthy controls from the TCGA dataset. We identified 67 transcription regulator genes whose expression is similar to the expression of both HSP90α and HSP90β across all of the cancer types studied (Figure 3B; Table S5). These co-expressed genes were not upregulated in all of the cancers, ruling out generic markers of cell proliferation. An independent approach using weighted gene co-expression network analysis (WGCNA; see Method Details) with a different statistical model identified 350 genes whose expression correlated with HSP90 (Table S6). Approximately two-thirds of 67 genes were also found in the set of 350 genes identified in WGCNA. For further work, we focused on these 67 genes, given the smaller number of genes compared to 350.

Core Functional Interactome of Nuclear HSP90

While individual hits obtained in each of the three datasets—genetic interactors, physical interactors, and cancer co-expression gene set—will be a valuable resource for future studies, we wanted to focus here on proteins that were identified in all three datasets. A pairwise comparison of the three datasets showed a high degree of overlap (Figure 3C), despite the fact that the three approaches were completely independent of one another. Five proteins were common to all three approaches used in our study: ACTL6, CHD4, HCFC1, RBBP4, and SMARCC2 (Figure 3D). The five genes identified as common to all three analyses were generally insensitive to the cutoff values used in each of the analyses, confirming the robustness of our conclusion (Figures S4C–S4E). We refer to these five proteins as the core functional interactome of nuclear HSP90 that interact with HSP90 both genetically and physically and are co-expressed with HSP90 in tumors. SMARCC2 and ACTL6 are part of the BRG1- or HBRM-associated factors (BAF) complex from the SWI/SNF chromatin remodeler family (Figure 3E). The SWI/SNF complex has been linked to HSP90 in independent studies in yeast (Zhao et al., 2005), validating our data. RBBP4 and CHD4 are part of the nucleosome remodeling deacetylase (NuRD) complex (Figure 3E), which is absent in budding yeast and has thus far not been connected with HSP90. Almost all of the members of the NuRD complex were identified in one or more of the three datasets described here (Figure 3E). Finally,

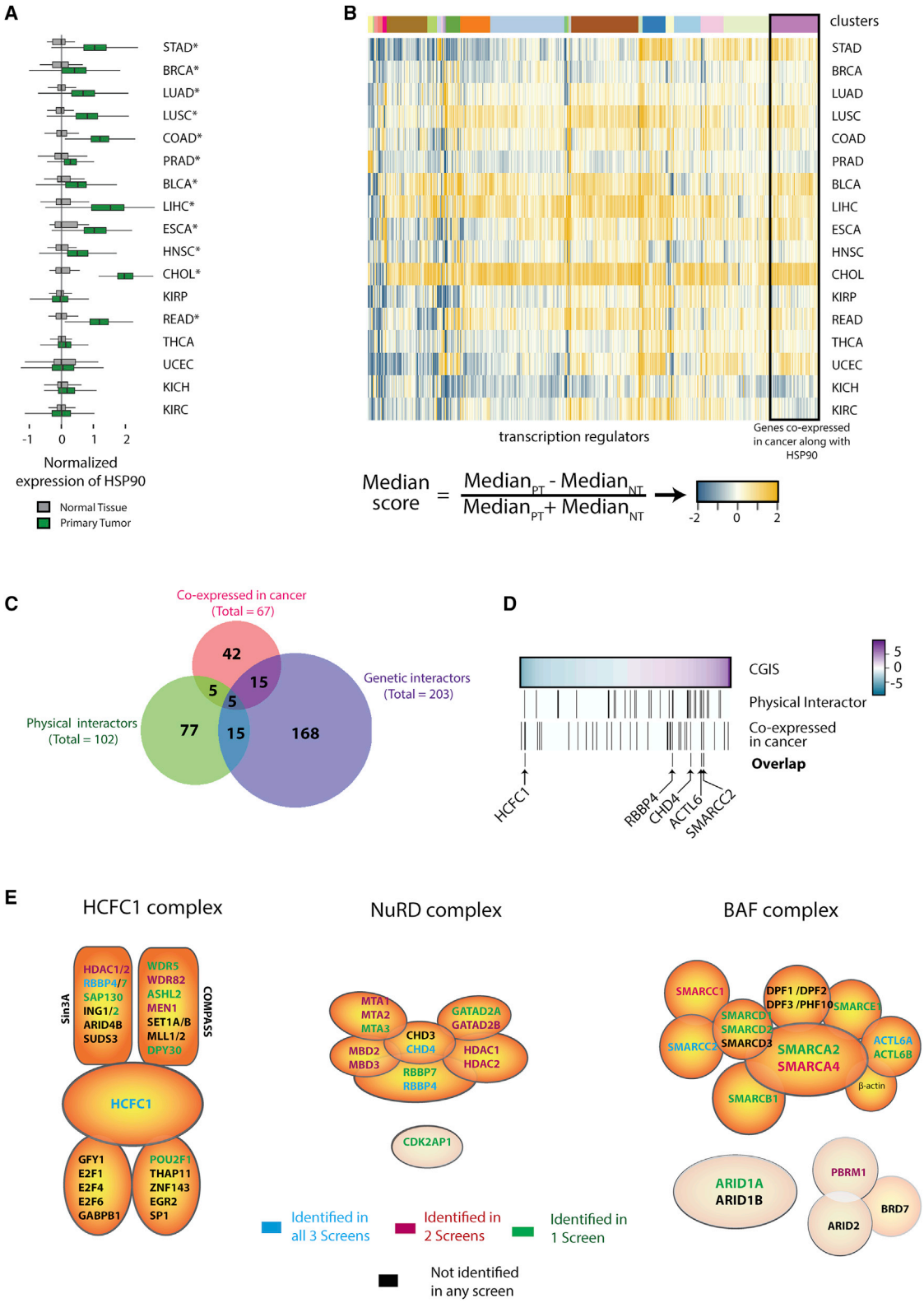

Figure 3. Core Functional Interactors of Nuclear HSP90

(A) Normalized expression levels of HSP90 in human RNA-seq datasets from The Cancer Genome Atlas (TCGA). Normal tissue is compared to primary tumors in 17 different cancer types. The dark line denotes the position of 0, the mean of normalized expression of HSP90 in normal tissues. The statistical significance of

(legend continued on next page)

metazoan-specific host cell factor C1 (HCFC1) was the only core functional interactor that showed negative genetic interaction with HSP90 (i.e., HCFC1 knockdown sensitizes cells to HSP90in) (Figures 1D and 3D). HCFC1, initially discovered as a host factor that supports the transcription of viral genes is a protein that is recruited to chromatin via a variety of transcription factors (TFs) and in turn acts as a platform to recruit chromatin modifying/remodeling complexes such as Sin3A histone deacetylase complex (HDAC) and Su(var)3-9, enhancer of zeste, trithorax/mixed lineage leukemia (MLL/SET) histone methyltransferase complex (Wysocka et al., 2003). Several members of the HCFC1 complex were recovered in one or more approaches used here (Figure 3E), suggesting a close molecular partnership between HSP90 and HCFC1. Thus, using a combination of orthogonal and independent approaches, we identified five proteins belonging to three different transcriptional complexes as core functional interactors of nuclear HSP90 (Figures 3D and 3E). To validate our findings in more detail at a mechanistic level, we further evaluated whether the core interactors require HSP90 for their gene-regulatory role at chromatin.

Genomic Analyses Identify HCFC1 as a Nuclear Target of HSP90

If HSP90 is required for the function or stability of an interactor X at chromatin, two predictions can be made: first, HSP90 and the interactor X should share genomic binding sites as evidenced by chromatin immunoprecipitation sequencing (ChIP-seq) co-occupancy, and second, HSP90 inhibition should lead to the loss of function of the interactor, causing misregulation specifically of the genes targeted by the interactor X. We tested both of these predictions in an unbiased manner. We used available ChIP-seq data of HSP90 in two human cell lines, K562 (Table S7) and BT474 (Greer et al., 2015), to identify the DNA sequence motifs enriched in the regions bound by HSP90. In addition, we analyzed promoter sequences of genes that are misregulated upon HSP90 inhibition using RNA-seq data of six different cell lines of human and mouse origin (either published in Hummel et al., 2017 or generated in the present study). Hypergeometric optimization of motif enrichment (HOMER)-based motif enrichment analyses of the promoter sequence (defined as −400 to +100 bp with transcription start site [TSS] at 0) of misregulated genes and HSP90 ChIP-seq peak regions identified 14 TF motifs (see Figure 4A; Method Details). We did not find the HSF1 motif in our analyses, despite the recent data linking HSP90 and HSF1 (Kijima et al., 2018). A detailed analysis revealed that the HSF1 motif was found only in the RNA-seq dataset when HSP90 inhibition was for a short duration (8 h), not a long duration (24 h). This is in line with the observation of HSF1 inactivation due to increased chaperone expression (Shi et al., 1998). Chaperone HSP70 upregulation in the early phase of HSP90 inhibition (2–8 h) likely dampens HSF1 activity in the later phases of HSP90 inhibition (24 h). Nonetheless, 7 of the 14 TFs that we identified (Figure 4A) are known to recruit HCFC1 to chromatin (Figure 3E), suggesting that HSP90 and HCFC1 may co-occupy genomic sites. ChIP-seq analyses confirmed that the binding sites of HSP90 overlap with the binding of HCFC1 and TFs known to recruit HCFC1 to chromatin (Michaud et al., 2013; Parker et al., 2014; Vogel and Kristie, 2000; Yu et al., 2010; Zargar and Tyagi, 2012; Figure 4B). A set of promoters not targeted by HSP90 acted as a negative control and showed no binding of HCFC1 (Figure 4B).

Having defined HCFC1 as a likely nuclear target of HSP90 in humans, we revisited the TCGA expression data to ask whether the components of the HCFC1 complex are co-expressed with HSP90 in cancers. We used the HCFC1 interactome that we manually curated by combining information from published data (Ajuh et al., 2000; Alfonso-Dunn et al., 2017; Deplus et al., 2013; Liu et al., 2010; Michaud et al., 2013; Parker et al., 2014; Wysocka et al., 2003; Yu et al., 2010; Table S8) and found that HSP90 expression is highly correlated with the expression of HCFC1 interactors in most cancer types (Figures 4C and S4F). We then analyzed the normalized RNA expression data of individual genes in primary tumors compared to corresponding normal tissues (Figure S5). Cancer types that show an increased RNA expression of HSP90 genes in tumors compared to normal tissues also showed an increased expression of HCFC1 interactors in tumors. The expression correlation between HSP90 and HCFC1 interactors held true even in protein expression data in colon adenocarcinoma for which quantitative protein abundance information was available for a few genes in the Clinical Proteome Tumor Analysis Consortium (CPTAC; Figure 4D). It is noteworthy that most of the HCFC1-interacting proteins were not used in the initial TCGA analysis described in Figure 3.

Thus, several independent approaches led us to suggest that nuclear HSP90 interacts with the metazoan-specific HCFC1-regulatory module. HCFC1 is 1 of the 11 genes called the death-from-cancer signature that were identified in a longitudinal study of ~1,000 cancer patients by Glinsky et al. (2005). Tumors that have high transcript levels of HCFC1 along with 10 other genes show poor therapeutic outcomes irrespective of the cancer type, which is reminiscent of the finding that NSCLC with high nuclear HSP90 levels shows poor prognosis (Su et al., 2016).

misregulation in cancer compared to normal tissue was determined by the Student's t test and indicated by asterisks. The acronyms of cancer types are in the standard form of TCGA (see Method Details).

(B) Heatmap showing the hierarchical clustering of 668 transcriptional regulators (Table S1) based on the median score of their expression across 17 different cancer types. The median score was calculated as indicated in the formula. $Median_{PT}$ and $median_{NT}$ denote the median expression of a gene in primary tumor (PT) and normal tissue (NT) samples. Clusters are indicated by colored boxes at top. The cluster containing HSP90AA1 and HSP90AB1 is highlighted with a black outline.

(C) Venn diagram showing the overlap between genetic interactors, physical interactors, and genes co-expressed with HSP90 in different cancer types.

(D) Five genes that were identified in all three screens are shown.

(E) Three complexes (BAF, NuRD, and HCFC1) are depicted with their respective subunits. The color scheme of the subunit names represent the number of screens in which the subunit was identified. Alternative subunits are shown in lighter-colored ovals. See Method Details for the subunit annotation sources. See also Figure S4 and Table S5.

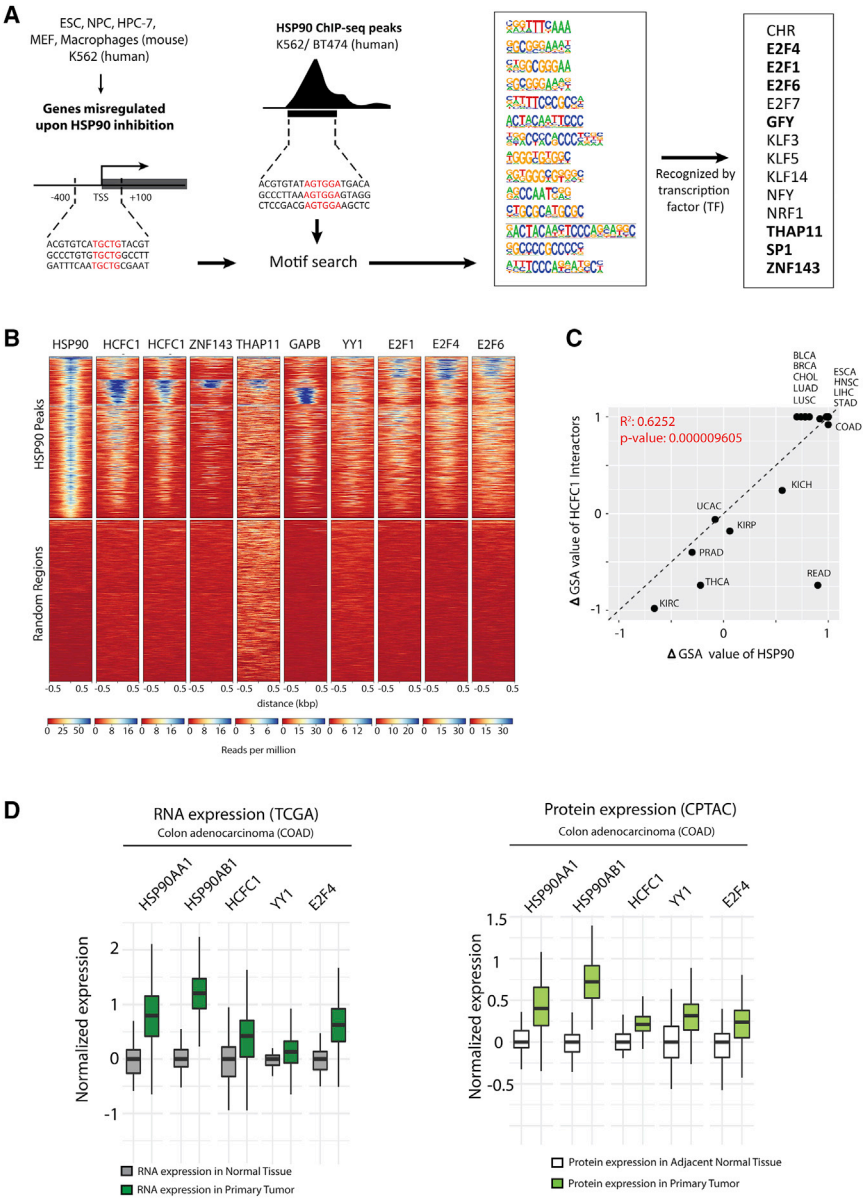

Figure 4. Physical and Function Interplay between HSP90 and HCFC1 at Chromatin

(A) Scheme to identify motifs underlying the function of HSP90 at chromatin. Promoter regions of genes misregulated upon HSP90 inhibition and HSP90 peak regions were used to identify enriched TF binding motifs. Names in bold indicate TFs known to recruit HCFC1 to chromatin (Figure 3F). The cell types used are indicated.

(B) ChIP-seq analysis for HSP90, HCFC1, and genes known to recruit HCFC1. Heatmaps visualize the occupancy of HSP90, HCFC1, ZNF143, THAP11, GAPB, YY1, E2F1, E2F4, and E2F6 in a 1,000-bp region around HSP90 peak summits and in HSP90-unbound promoter regions. HSP90 ChIP-seq was done in K562 cells; all of the other data are from HeLa cells. Color-scaled ChIP-seq read intensities are in units of reads per million (RPM).

(C) Gene set analysis (GSA) of the gene expression levels in primary tumor samples compared to normal tissue samples based on RNA-seq datasets from TCGA. Known HCFC1 interactors (Table S8) are grouped in one gene set (y axis). The significance of the up- or downregulation of genes in primary tumors versus normal tissues is calculated as ΔGSA value. The maximal significance of upregulation is indicated by +1 (p = 0), while the maximal significance of downregulation is indicated by −1 (p = 0). ΔGSA values for HSP90 are plotted against ΔGSA values of HCFC1 interactors in the scatterplot, with each dot representing one cancer type in TCGA. R^2 and p values calculated using a linear regression analysis are shown.

(D) Normalized expression levels of HSP90, HCFC1, and two proteins known to recruit HCFC1 in samples of normal tissue in comparison with primary tumors in colon adenocarcinoma. Source data: RNA expression from TCGA (left) and protein expression from CPTAC (right; see Method Details). Boxplots display the 25th to the 75th percentiles (boxes), the median is shown by the middle line, and the whiskers depict 1.5 times the interquartile range. See Figure S5 for all other cancer datasets.

See also Figures S4 and S5 and Tables S6, S7, and S8.

Stabilization of HCFC1 by HSP90 Is Required for Cell-Cycle Gene Expression

We tested the possibility that nuclear HSP90 chaperones and stabilizes HCFC1 against misfolding and degradation. HCFC1 is a large protein of ~300 kDa and is proteolytically processed into N- and C-terminal fragments of ~150 kDa each (Capotosti et al., 2011). These two forms of HCFC1 bind chromatin at the same promoters tethered by various TFs (Michaud et al., 2013). Upon HSP90 inhibition, protein levels of uncleaved HCFC1 and its N- and C-terminal fragments are drastically reduced, without having much effect on HCFC1 transcript levels (Figures 5A and S6A). Cytosolic levels of HCFC1 levels were not altered by HSP90 inhibition, even at the HSP90in concentration that leads to the degradation of other known clients of HSP90 (Basso et al., 2002; Ding et al., 2016; Walerych et al., 2004) and the transcriptional upregulation of chaperones as expected (Figures S6B–S6D). The degradation of HCFC1 upon HSP90 inhibition depended on functional autophagy, but not the proteasome pathway (Figures S6E and S6F), which is in line with a recent report for another transcriptional regulator (Wang et al., 2018).

Next, we assessed whether HSP90 inhibition causes the misregulation of HCFC1 targets, as can be expected from the decrease in chromatin-associated HCFC1. As observed in publicly available RNA-seq data (Hummel et al., 2017), acute HSP90 inhibition in mouse embryonic stem cells (ESCs) causes the transcriptional upregulation of 2,727 genes and the downregulation of 1,539 genes ($p < 0.01$, absolute fold change >2). Mainly downregulated genes were targeted by HCFC1 at their promoters, but not upregulated genes (Figures 5B and S7A). A network analysis

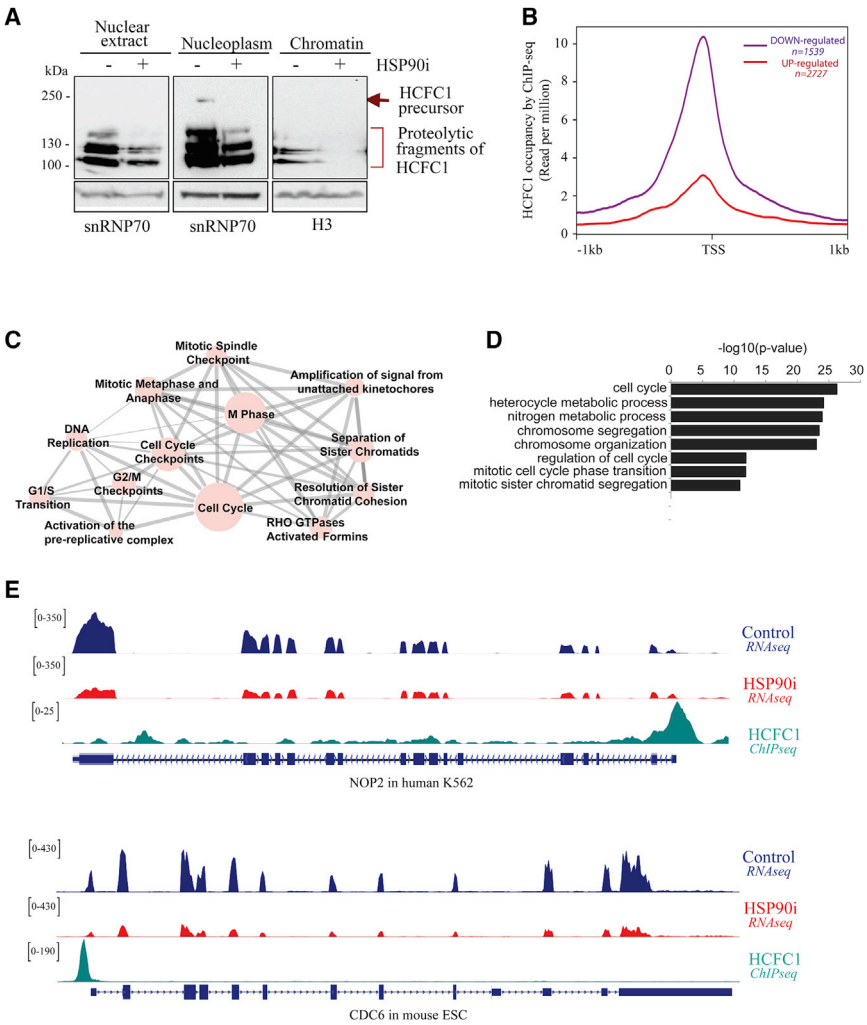

Figure 5. HSP90 Controls Cell-Cycle Gene Expression by Stabilizing HCFC1

(A) HSP90 inhibition leads to HCFC1 protein level decrease in total nuclear extracts, nucleoplasm, and chromatin fractions in HEK293 cells. snRNP70 and H3 served as loading controls. The control experiments to validate HSP90 inhibition are shown in Figures S6C and S6D.

(B) Metaplots of HCFC1 binding around transcriptional start sites (TSSs) of downregulated (purple) and upregulated (red) genes in mouse ESCs (mESCs) upon HSP90 inhibition. The y axes indicate normalized ChIP-seq occupancy in RPM.

(C) Enrichment map of Reactome pathways defined by genes that are HCFC1 targets and are downregulated upon HSP90 inhibition. Node size represents the number of downregulated genes that overlap with the corresponding Reactome pathway, and the size of the edges represent the number of shared genes between two connecting pathways.

(D) List of biological processes defined by Gene Ontology for genes that are HCFC1 targets and are downregulated upon HSP90 inhibition. p values assessed by Fisher's exact test with multiple-test correction are shown.

(E) Genome browser tracks of two representative genes: NOP2 in K562 cells (top panel) and CDC6 in mESCs (bottom panel). ChIP-seq occupancy of HCFC1 at promoters is shown in cyan. Expression levels are visualized in control conditions (blue) and upon HSP90 inhibition (red). The vertical scale indicates normalized read density in RPM.

See also Figures S6 and S7.

of genes targeted by HCFC1 that are downregulated upon HSP90 inhibition showed an enrichment of the regulators of the cell cycle and chromosome segregation (Figures 5C and 5D; e.g., proliferating cell nucleolar antigen NOP2 and cell-division cycle 6 [CDC6]; Figure 5E). HSP90 inhibition causes a significantly stronger downregulation of HCFC1-targeted cell-cycle genes as compared to HCFC1-non-targeted cell-cycle genes (Figure S7B). We selected a short list of cell-cycle genes that are cancer relevant and some of which are being considered for cancer therapeutics (Figure S7C). Using qPCR analyses, we confirmed that HSP90 inhibition causes the downregulation of these cell-cycle genes to varying degrees (Figure S7D). More important, the overexpression of HCFC1 rescued the downregulation caused by HSP90 inhibition (Figure S7D), further suggesting that HSP90 regulates the expression of these genes by stabilizing HCFC1.

Interaction between HCFC1 and HSP90 Is Important for Diverse Cellular Processes

To further test the role of chaperoning HCFC1 function by HSP90 in maintaining gene expression, we used multiple independent models. In the first model, we asked whether the HSP90-HCFC1 interaction is important for the proliferation of K562 cells. Analogous to the chemical-genetic screen (Figure 1), we quantified the effect of HSP90in on K562 cells with or without knock down of HCFC1. Control knock down of renilla luciferase did not sensitize cells to HSP90 inhibition. HCFC1 depletion, however, exacerbated the effect of HSP90in on cell viability (Figure 6A), confirming our results with the chemical-genetic screen. To further strengthen the evidence that HSP90 physically and functionally interacts with HCFC1, we used the biochemical approach of co-immunoprecipitation using truncated forms of HCFC1. HSP90 was found to interact with the N-terminal fragment of HCFC1, specifically the Kelch domain but not the C-terminal fragment (Figures 6B and S8A). Due to expression differences between N- and C-terminal fragments of tagged HCFC1, it is difficult to reach a conclusion about their relative HSP90 interaction strength. Moreover, we found that the client-trapping mutant of HSP90, E42A (Prince et al., 2015), interacts with a higher affinity with the HCFC1 N-terminal and Kelch domains (Figure S8B), further confirming that HCFC1 is a client of HSP90. To genetically test the interaction between the Kelch domain and HSP90, we capitalized on a known spontaneous point mutation in the Kelch domain of HCFC1, P134S, originally isolated from the hamster cell line BHK-21 (Goto et al., 1997).

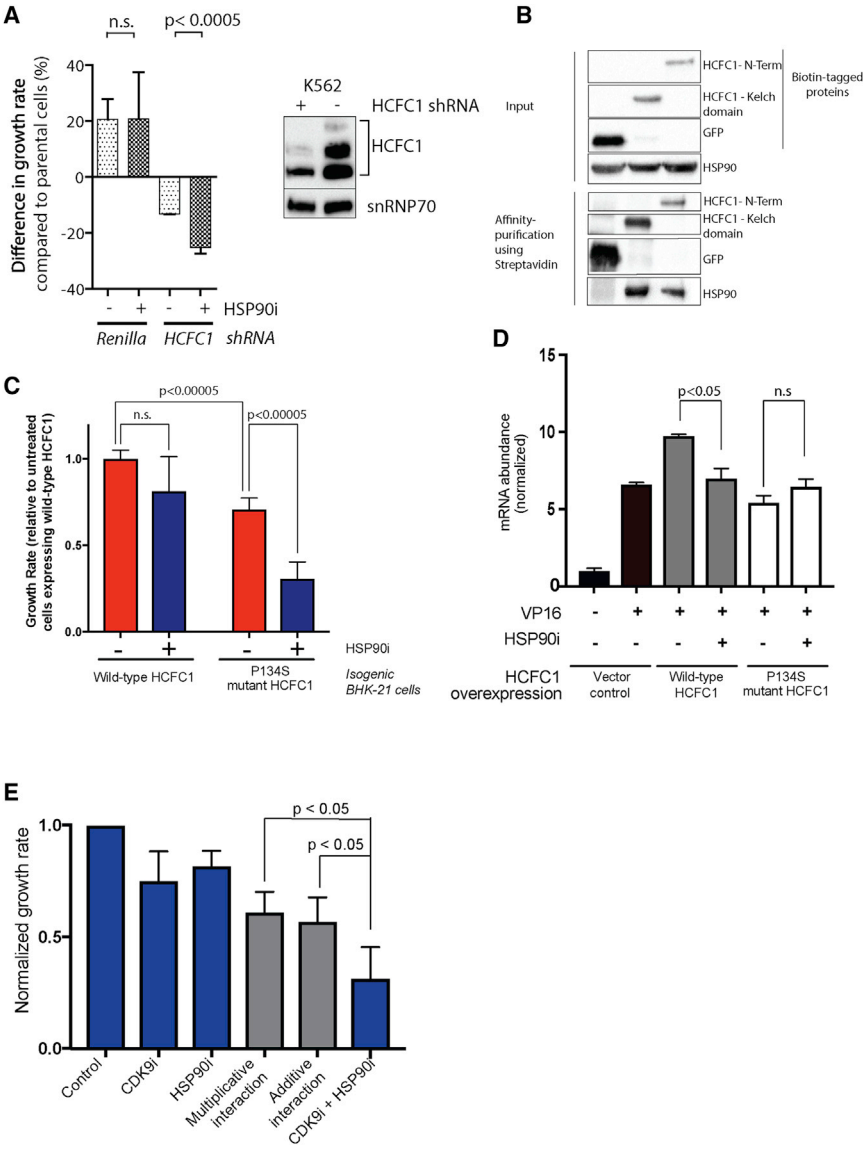

Figure 6. Functional Relevance of HSP90-HCFC1 Interaction Assessed in Independent Cellular Models

(A) Effect of HCFC1 knockdown on the mean growth rate of K562 cells in the presence and absence of HSP90in as measured by growth competition assay. Inset: western blot analysis of HCFC1 upon knock down, with shRNA directed against HCFC1. For normalization, snRNP70 was used.

(B) Hsp90 co-purification upon affinity pull down of the HCFC1 Kelch domain or the HCFC1 N-terminal fragment in HeLa cells.

(C) Effect of a point mutation P134S in the Kelch domain of HCFC1 sensitizes cells to HSP90 inhibition. Two isogenic BHK-21 cell lines differing in one residue of HCFC1 (mutant and wild type) were exposed to HSP90 inhibition, and the effect on growth was determined. The statistical significance was calculated using the one-tailed t test. The mean growth rate with SD is shown for three replicates.

(D) Effect of HSP90 inhibitor and HCFC1 overexpression on VP16-induced transcription of viral promoter-reporter constructs. Normalized values of mRNA abundance of the reporter as evaluated by qRT-PCR are shown as means and SEMs. The effect of wild-type and P134S mutant HCFC1 overexpression are shown. The statistical significance was calculated using the one-tailed t test.

(E) Effect of CDK9 and HSP90 inhibitors either individually or in combination on the growth rate of myeloma cell line U266. The mean growth rate with SEM is shown for three replicates. The gray bars indicate the expected outcome of growth rates if the two inhibitors worked additively or by multiplicative interaction. The experimental outcome of the combination treatment is significantly lower than that of the expected outcome, as shown by the p values (one-tailed t test).

See also Figures S8 and S9.

This model allowed us to compare the effect of the HSP90 inhibitor on two isogenic cell lines that differ in only one residue of HCFC1. While HSP90 inhibition only mildly affected the growth rate of wild-type cells, mutant cells were significantly sensitive to HSP90 inhibition (Figure 6C), confirming the requirement of HSP90 for optimal HCFC1 function in driving cell proliferation. We found that the steady-state protein levels of the HCFC1-P134S mutant are lower than those of the wild-type HCFC1 (Figure S8C). Furthermore, mutant protein, especially the full-length HCFC1, bound with much higher affinity to HSP90 as compared to wild type (Figure S8D). These data suggest that the P134S mutant HCFC1 is highly unstable and is much more dependent on HSP90, which is in line with the finding that HSP90 binds to the Kelch domain where the mutation P134S lies.

In the second model, we studied the ability of HCFC1 to activate the transcription of the immediate early (IE) promoter of the herpes simplex virus (HSV). IE promoter expression is driven by the viral protein 16 (VP16) that recruits HCFC1 (Wysocka and Herr, 2003). We found that the activity of the HSV-IE promoter is increased by VP16 expression as expected (Figure 6D). Co-expression of wild-type HCFC1 but not P134S mutant HCFC1 caused a further increase in the HSV-IE reporter, which was sensitive to HSP90 inhibition (Figure 6D). Hence, HCFC1 requires HSP90 for activating transcription from viral promoters, which is in line with the observation that cellular promoters targeted by HCFC1 are downregulated upon HSP90 inhibition (Figures 5B and 5E).

Simultaneous Inhibition of CDK9 and HSP90 Suppresses Cell Proliferation

Using three orthogonal analyses combined with genomic and biochemical analyses, our study uncovered the importance of the collaboration between HSP90 and HCFC1 in driving cell-cycle gene expression fueling proliferation. Thus, simultaneous inhibition of HSP90 and HCFC1 function should prove to be synergistically lethal for cancer cells, similar to pharmacological

synergy (Loewe, 1953). Our chemical-genetic screen already identified HCFC1 as one of the proteins that when knocked down makes cells highly sensitive to Hsp90in (Figures 1D and 1E). HCFC1 itself cannot be targeted by small molecule inhibitors such as HSP90, limiting the practical application of our findings to cancer treatment. Hence, we sought to identify HCFC1 interactors that also bind to HSP90 and can be targeted by small molecules. Comparing HCFC1 interactors (Table S8) with HSP90 interactors (Table S4), we identified cyclin-dependent kinase 9 (CDK9) as a potential candidate. CDK9 is recruited by HCFC1 to viral promoters for the activation of IE genes (Alfonso-Dunn et al., 2017). Small-molecule inhibitors of CDK9 block the expression of these viral genes (Alfonso-Dunn et al., 2017), similar to HSP90 inhibitors (Figure 6E). HSP90 has independently been shown to interact with CDK9 (O'Keeffe et al., 2000), likely in association with HCFC1. We directly tested whether HSP90in could synergize with CDK9 inhibitors (CDK9is) in killing cancer cells. CDK9i worked optimally to reduce the expression of target cell-cycle genes, as expected (Figure S9A; Aprile-Garcia et al., 2019). While individual inhibitors had only a mild effect on proliferation, a combination of these two inhibitors showed synergistic lethal effects on the cell proliferation of myeloma cell line U266 (Figure 6E). The combination was more effective than expected for an additive or multiplicative interaction between the two inhibitors (Baryshnikova et al., 2013). The simultaneous inhibition caused a substantial increase in the fraction of apoptotic cells and an enhanced proportion of cells in G0 phase of the cell cycle (Figure S9B), phenocopying the loss of function of HCFC1 (Goto et al., 1997).The simultaneous inhibition caused a more persistent and severe decrease in the expression of cell-cycle genes (Figure S9C). We further tested a more potent and specific CDK9 inhibitor that was recently developed, MC180295 (Zhang et al., 2018) for its synergy with HSP90 inhibitor in U266, K562, and HeLa cells. In all of the cases tested, MC180295 was synergistic with HSP90in in controlling the proliferation of cells (Figure S9D). In summary, the identification of HCFC1 in this study as a target of nuclear HSP90 can be harnessed to provide a combination of drugs targeting proteostasis and transcription.

DISCUSSION

Proteins that have completed *de novo* folding enter the nucleus to encounter a unique challenge of dealing with chromatin polymers. Our understanding of nuclear protein quality control still requires a global understanding of chaperone clients in this cellular compartment. By using three orthogonal and independent approaches, this study provides a global analysis of the nuclear pool of HSP90 in human cells. We used different cell lines and cancer types for implementing the diverse approaches with the aim of identifying fundamental, cell-type-invariant regulatory modules that are chaperoned by HSP90.

The individual approaches detailed in this work will be a rich resource for follow-up studies. For example, expression of the interacting genes (Figure 1) in tumors treated with HSP90in may predict therapeutic responsiveness among patients. In this regard, it is noteworthy that we identified the SWI/SNF complex in multiple analyses described here. Mutations in SWI/SNF components have been recently linked to the sensitivity of tumors to immunotherapy (Miao et al., 2018; Pan et al., 2018), suggesting that HSP90 inhibitors may be synergistically combined with immune checkpoint blockade. Similarly, HDACs recovered in our work have already proved to be successful when combined with HSP90in in cancer treatment (Krämer et al., 2014). It is likely that HSP90 is critical for the assembly and/or the function of BAF and NuRD complexes in the nucleus, both of which are important cancer modifiers. It should be noted that most available HSP90 inhibitors are likely to inhibit both cytosolic and nuclear HSP90, affecting the levels of chromatin regulators in both of these compartments.

The protein quality control mechanism controlled by HSP90 works in unison with co-chaperones and E3 ubiquitin ligases. Besides HSP70, we found kinase-specific co-chaperone CDC37 in the nuclear interactome of HSP90, along with multiple kinases. We found that HCFC1 degradation upon HSP90 inhibition depends on autophagy rather than the proteasome. How nuclear proteins are carried to autophagosomes will be an important question for future studies. It is not clear how HSP90 selects its clients in the nucleus, where all of the proteins have already finished the initial aspects of folding and maturation. Some common themes have emerged from work of the last few years. Three clients of HSP90, namely HCFC-1, trithorax/MLL, and picornavirus capsid precursor poly-protein (P1), undergo proteolytic processing as a part of their functional maturation (Geller et al., 2007; Tariq et al., 2009). It is possible that a common quality control feature associated with the proteolytic maturation of proteins requires HSP90. In addition, we recently reported the identification of the TRIM28 complex as a nuclear client of HSP90 (Hummel et al., 2017), which can be recapitulated in our work here (Figure 2E; Tables S3 and S4). TRIM28 and HCFC1 are both metazoan specific and act as a bridging platform between TFs and chromatin-modifying proteins. It is likely that the structural complexity of such a platform necessitates chaperone action and control. The molecular determinants by which HSP90 controls these platforms will be an exciting area of future studies.

HCFC1 was named after its function as a host factor necessary for the activation of viral IE promoters via binding VP16. The finding that HCFC1 critically requires HSP90 for its stability suggests that viral transcription and propagation in host cells will be sensitive to HSP90 inhibition. Thus, HSP90 constitutes an important host protein required for viral transcription and replication (Geller et al., 2012; Wang et al., 2018), and HSP90 inhibitors could be used as broad antiviral agents (Wang et al., 2017).

The premise of the use of HSP90 inhibitors in cancer therapy is based on the findings that cancer cells are more sensitive to HSP90in than untransformed normal cells. A recent study implicated cellular quiescence and activity as a likely cause for the differential sensitivity of normal and cancer cells to HSP90in (Echeverria et al., 2019). The cellular activity of cancer cells is driven by proliferation and the cell cycle. HSP90 is known to directly stabilize multiple cell-cycle proteins. Our finding that HSP90 regulates the transcription of cell-cycle genes defines yet another layer of cell-cycle control by HSP90, likely contributing to the heightened sensitivity of cancer cells to HSP90in.

TCGA data confirmed the previous findings that HSP90 is transcriptionally upregulated in several cancer samples. It is not clear how the expression of HSP90 is coordinated with that of its interactors at the level of transcription, as we found in our cancer co-expression analyses. One possibility is that proliferating cells are fueled by the increased expression of cell-cycle regulators such as HCFC1, which may enhance proteostatic demands. Such demands may activate the HSF pathway, causing a transcriptional upregulation of HSP90 genes. Nonetheless, the data presented here suggest that HSP90 inhibitors can be rationally combined with drugs that target transcription to enhance their therapeutic potential. In summary, our study provides global insights into the function of nuclear HSP90 in human cells, suggesting therapeutic intervention strategies that will bolster attempts to make HSP90 inhibitors more effective in clinical settings.

STAR★METHODS

Detailed methods are provided in the online version of this paper and include the following:

- KEY RESOURCES TABLE
- LEAD CONTACT AND MATERIALS AVAILABILITY
- EXPERIMENTAL MODEL AND SUBJECT DETAILS
- METHOD DETAILS
  - Chemical-Genetic Interaction Screen
  - Cell Fractionation
  - SDS-PAGE
  - Silver Staining
  - Western Blotting
  - Nuclear Protein Affinity Purification Coupled to Mass Spectrometry
  - RNA Isolation
  - ChIP-Seq
  - Biochemical Analyses of Protein Stability and Interactions
  - Experiments Testing Functional Interaction between HSP90 and HCFC1
  - RNA-Seq
- QUANTIFICATION AND STATISTICAL ANALYSIS
  - Computational Analysis of Sequencing Data
  - Gene Set Analysis (GSA)
  - Protein Expression Visualization
  - Motif Discovery
  - Statistical Tests
- DATA AND CODE AVAILABILITY

SUPPLEMENTAL INFORMATION

Supplemental Information can be found online at https://doi.org/10.1016/j.celrep.2019.09.084.

ACKNOWLEDGMENTS

We would like to thank Winship Herr (University of Lausanne, Lausanne, Switzerland), Prof. Takeharu Nishimoto (Kyushu University, Fukuoka, Japan), Monika Engelhardt (University Clinic Freiburg, Freiburg, Germany), Jean-Pierre Issa (Temple University, Philadelphia, PA, USA), Christos A. Panagiotidis (Aristotle University of Thessaloniki, Thessaloniki, Greece), and Thomas Jenuwein and Eirini Trompouki (Max Planck Institute for Immunobiology and Epigenetics, Freiburg, Germany) for sharing cell lines, inhibitors, protocols, and plasmids. This work was financially supported by the Max Planck Society, German Research Foundation (DFG) through the collaborative research center CRC992 (Medical Epigenetics), via the research grant SA 3190 and through Germany's Excellence Strategy (CIBSS – EXC-2189 – Project ID 390939984) to R.S. C.M. acknowledges financial support from the German Cancer Consortium (DKTK).

AUTHOR CONTRIBUTIONS

R.S. conceived the project and designed the study; A.A., D.M.R., F.A.-G., P.R., E.C.H., A.K., and K.G. performed the experiments and interpreted the results; B.H., M.S., J.M., G.M., and C.M. performed the computational analyses; and R.S. wrote the manuscript with input from all of the authors.

DECLARATION OF INTERESTS

The authors declare no competing interests.

Received: March 19, 2019
Revised: August 6, 2019
Accepted: September 27, 2019
Published: November 5, 2019

REFERENCES

Ajuh, P.M., Browne, G.J., Hawkes, N.A., Cohen, P.T., Roberts, S.G., and Lamond, A.I. (2000). Association of a protein phosphatase 1 activity with the human factor C1 (HCF) complex. Nucleic Acids Res. *28*, 678–686.

Alfonso-Dunn, R., Turner, A.W., Jean Beltran, P.M., Arbuckle, J.H., Budayeva, H.G., Cristea, I.M., and Kristie, T.M. (2017). Transcriptional Elongation of HSV Immediate Early Genes by the Super Elongation Complex Drives Lytic Infection and Reactivation from Latency. Cell Host Microbe *21*, 507–517.e5.

Aprile-Garcia, F., Tomar, P., Hummel, B., Khavaran, A., and Sawarkar, R. (2019). Nascent-protein ubiquitination is required for heat shock-induced gene downregulation in human cells. Nat. Struct. Mol. Biol. *26*, 137–146.

Arrigoni, L., Richter, A.S., Betancourt, E., Bruder, K., Diehl, S., Manke, T., and Bönisch, U. (2016). Standardizing chromatin research: a simple and universal method for ChIP-seq. Nucleic Acids Res. *44*, e67.

Bao, Y., and Shen, X. (2007). SnapShot: chromatin remodeling complexes. Cell *129*, 632.

Baryshnikova, A., Costanzo, M., Myers, C.L., Andrews, B., and Boone, C. (2013). Genetic interaction networks: toward an understanding of heritability. Annu. Rev. Genomics Hum. Genet. *14*, 111–133.

Basso, A.D., Solit, D.B., Chiosis, G., Giri, B., Tsichlis, P., and Rosen, N. (2002). Akt forms an intracellular complex with heat shock protein 90 (Hsp90) and Cdc37 and is destabilized by inhibitors of Hsp90 function. J. Biol. Chem. *277*, 39858–39866.

Berbers, G.A., Kunnen, R., van Bergen en Henegouwen, P.M., and van Wijk, R. (1988). Localization and quantitation of hsp84 in mammalian cells. Exp. Cell Res. *177*, 257–271.

Bohenzky, R.A., Papavassiliou, A.G., Gelman, I.H., and Silverstein, S. (1993). Identification of a promoter mapping within the reiterated sequences that flank the herpes simplex virus type 1 UL region. J. Virol. *67*, 632–642.

Brough, P.A., Aherne, W., Barril, X., Borgognoni, J., Boxall, K., Cansfield, J.E., Cheung, K.M., Collins, I., Davies, N.G., Drysdale, M.J., et al. (2008). 4,5-diarylisoxazole Hsp90 chaperone inhibitors: potential therapeutic agents for the treatment of cancer. J. Med. Chem. *51*, 196–218.

Calderwood, S.K., and Neckers, L. (2016). Hsp90 in Cancer: Transcriptional Roles in the Nucleus. In Advances in Cancer Research, I. Jennifer and W. Luke, eds. (Academic Press), pp. 89–106.

Canonici, A., Qadir, Z., Conlon, N.T., Collins, D.M., O'Brien, N.A., Walsh, N., Eustace, A.J., O'Donovan, N., and Crown, J. (2018). The HSP90 inhibitor NVP-AUY922 inhibits growth of HER2 positive and trastuzumab-resistant breast cancer cells. Invest. New Drugs *36*, 581–589.

Capotosti, F., Guernier, S., Lammers, F., Waridel, P., Cai, Y., Jin, J., Conaway, J.W., Conaway, R.C., and Herr, W. (2011). O-GlcNAc transferase catalyzes site-specific proteolysis of HCF-1. Cell *144*, 376–388.

Colaprico, A., Silva, T.C., Olsen, C., Garofano, L., Cava, C., Garolini, D., Sabedot, T.S., Malta, T.M., Pagnotta, S.M., Castiglioni, I., et al. (2016). TCGAbiolinks: an R/Bioconductor package for integrative analysis of TCGA data. Nucleic Acids Res. *44*, e71.

Cox, J., Hein, M.Y., Luber, C.A., Paron, I., Nagaraj, N., and Mann, M. (2014). Accurate proteome-wide label-free quantification by delayed normalization and maximal peptide ratio extraction, termed MaxLFQ. Mol. Cell. Proteomics *13*, 2513–2526.

Cvoro, A., Tzagarakis-Foster, C., Tatomer, D., Paruthiyil, S., Fox, M.S., and Leitman, D.C. (2006). Distinct roles of unliganded and liganded estrogen receptors in transcriptional repression. Mol. Cell *21*, 555–564.

Deeb, S.J., Cox, J., Schmidt-Supprian, M., and Mann, M. (2014). N-linked glycosylation enrichment for in-depth cell surface proteomics of diffuse large B-cell lymphoma subtypes. Mol. Cell. Proteomics *13*, 240–251.

Deplus, R., Delatte, B., Schwinn, M.K., Defrance, M., Méndez, J., Murphy, N., Dawson, M.A., Volkmar, M., Putmans, P., Calonne, E., et al. (2013). TET2 and TET3 regulate GlcNAcylation and H3K4 methylation through OGT and SET1/COMPASS. EMBO J. *32*, 645–655.

Dignam, J.D., Lebovitz, R.M., and Roeder, R.G. (1983). Accurate transcription initiation by RNA polymerase II in a soluble extract from isolated mammalian nuclei. Nucleic Acids Res. *11*, 1475–1489.

Ding, G., Chen, P., Zhang, H., Huang, X., Zang, Y., Li, J., Li, J., and Wong, J. (2016). Regulation of Ubiquitin-like with Plant Homeodomain and RING Finger Domain 1 (UHRF1) Protein Stability by Heat Shock Protein 90 Chaperone Machinery. J. Biol. Chem. *291*, 20125–20135.

Eccles, S.A., Massey, A., Raynaud, F.I., Sharp, S.Y., Box, G., Valenti, M., Patterson, L., de Haven Brandon, A., Gowan, S., Boxall, F., et al. (2008). NVP-AUY922: a novel heat shock protein 90 inhibitor active against xenograft tumor growth, angiogenesis, and metastasis. Cancer Res. *68*, 2850–2860.

Echeverría, P.C., Bernthaler, A., Dupuis, P., Mayer, B., and Picard, D. (2011). An interaction network predicted from public data as a discovery tool: application to the Hsp90 molecular chaperone machine. PLoS One *6*, e26044.

Echeverria, P.C., Bhattacharya, K., Joshi, A., Wang, T., and Picard, D. (2019). The sensitivity to Hsp90 inhibitors of both normal and oncogenically transformed cells is determined by the equilibrium between cellular quiescence and activity. PLoS One *14*, e0208287.

Echtenkamp, F.J., Gvozdenov, Z., Adkins, N.L., Zhang, Y., Lynch-Day, M., Watanabe, S., Peterson, C.L., and Freeman, B.C. (2016). Hsp90 and p23 Molecular Chaperones Control Chromatin Architecture by Maintaining the Functional Pool of the RSC Chromatin Remodeler. Mol. Cell *64*, 888–899.

Efron, B., and Tibshirani, R. (2007). On testing the significance of sets of genes. Ann. Appl. Stat. *1*, 107–129.

Engelke, R., Riede, J., Hegermann, J., Wuerch, A., Eimer, S., Dengjel, J., and Mittler, G. (2014). The quantitative nuclear matrix proteome as a biochemical snapshot of nuclear organization. J. Proteome Res. *13*, 3940–3956.

Falsone, S.F., Gesslbauer, B., Tirk, F., Piccinini, A.M., and Kungl, A.J. (2005). A proteomic snapshot of the human heat shock protein 90 interactome. FEBS Lett. *579*, 6350–6354.

Falsone, S.F., Gesslbauer, B., Rek, A., and Kungl, A.J. (2007). A proteomic approach towards the Hsp90-dependent ubiquitinylated proteome. Proteomics *7*, 2375–2383.

Freeman, B.C., and Yamamoto, K.R. (2002). Disassembly of transcriptional regulatory complexes by molecular chaperones. Science *296*, 2232–2235.

Gano, J.J., and Simon, J.A. (2010). A proteomic investigation of ligand-dependent HSP90 complexes reveals CHORDC1 as a novel ADP-dependent HSP90-interacting protein. Mol. Cell. Proteomics *9*, 255–270.

Geller, R., Vignuzzi, M., Andino, R., and Frydman, J. (2007). Evolutionary constraints on chaperone-mediated folding provide an antiviral approach refractory to development of drug resistance. Genes Dev. *21*, 195–205.

Geller, R., Taguwa, S., and Frydman, J. (2012). Broad action of Hsp90 as a host chaperone required for viral replication. Biochim. Biophys. Acta *1823*, 698–706.

Glinsky, G.V., Berezovska, O., and Glinskii, A.B. (2005). Microarray analysis identifies a death-from-cancer signature predicting therapy failure in patients with multiple types of cancer. J. Clin. Invest. *115*, 1503–1521.

Goto, H., Motomura, S., Wilson, A.C., Freiman, R.N., Nakabeppu, Y., Fukushima, K., Fujishima, M., Herr, W., and Nishimoto, T. (1997). A single-point mutation in HCF causes temperature-sensitive cell-cycle arrest and disrupts VP16 function. Genes Dev. *11*, 726–737.

Greer, C.B., Tanaka, Y., Kim, Y.J., Xie, P., Zhang, M.Q., Park, I.-H., and Kim, T.H. (2015). Histone deacetylases positively regulate transcription through the elongation machinery. Cell Rep. *13*, 1444–1455.

Gvozdenov, Z., Kolhe, J., and Freeman, B.C. (2019). The Nuclear and DNA-Associated Molecular Chaperone Network. Cold Spring Harb. Perspect. Biol. *11*, a034009.

Hadizadeh Esfahani, A., Sverchkova, A., Saez-Rodriguez, J., Schuppert, A.A., and Brehme, M. (2018). A systematic atlas of chaperome deregulation topologies across the human cancer landscape. PLoS Comput. Biol. *14*, e1005890.

Hartl, F.U. (1996). Molecular chaperones in cellular protein folding. Nature *381*, 571–579.

Hauri, S., Comoglio, F., Seimiya, M., Gerstung, M., Glatter, T., Hansen, K., Aebersold, R., Paro, R., Gstaiger, M., and Beisel, C. (2016). A High-Density Map for Navigating the Human Polycomb Complexome. Cell Rep. *17*, 583–595.

Heinz, S., Benner, C., Spann, N., Bertolino, E., Lin, Y.C., Laslo, P., Cheng, J.X., Murre, C., Singh, H., and Glass, C.K. (2010). Simple combinations of lineage-determining transcription factors prime cis-regulatory elements required for macrophage and B cell identities. Mol. Cell *38*, 576–589.

Hulsen, T., de Vlieg, J., and Alkema, W. (2008). BioVenn - a web application for the comparison and visualization of biological lists using area-proportional Venn diagrams. BMC Genomics *9*, 488.

Hummel, B., Hansen, E.C., Yoveva, A., Aprile-Garcia, F., Hussong, R., and Sawarkar, R. (2017). The evolutionary capacitor HSP90 buffers the regulatory effects of mammalian endogenous retroviruses. Nat. Struct. Mol. Biol. *24*, 234–242.

Isaacs, J.S. (2016). Hsp90 as a "Chaperone" of the Epigenome: Insights and Opportunities for Cancer Therapy. In Advances in Cancer Research, I. Jennifer and W. Luke, eds. (Academic Press), pp. 107–140.

Kasten, M.M., Clapier, C.R., and Cairns, B.R. (2011). SnapShot: chromatin remodeling: SWI/SNF. Cell *144*, 310.e1.

Kijima, T., Prince, T.L., Tigue, M.L., Yim, K.H., Schwartz, H., Beebe, K., Lee, S., Budzynski, M.A., Williams, H., Trepel, J.B., et al. (2018). HSP90 inhibitors disrupt a transient HSP90-HSF1 interaction and identify a noncanonical model of HSP90-mediated HSF1 regulation. Sci. Rep. *8*, 6976.

Kim, D., Pertea, G., Trapnell, C., Pimentel, H., Kelley, R., and Salzberg, S.L. (2013). TopHat2: accurate alignment of transcriptomes in the presence of insertions, deletions and gene fusions. Genome Biol. *14*, R36.

Krämer, O.H., Mahboobi, S., and Sellmer, A. (2014). Drugging the HDAC6-HSP90 interplay in malignant cells. Trends Pharmacol. Sci. *35*, 501–509.

Langfelder, P., and Horvath, S. (2008). WGCNA: an R package for weighted correlation network analysis. BMC Bioinformatics *9*, 559.

Langmead, B., and Salzberg, S.L. (2012). Fast gapped-read alignment with Bowtie 2. Nat. Methods *9*, 357–359.

Lee, T.I., Johnstone, S.E., and Young, R.A. (2006). Chromatin immunoprecipitation and microarray-based analysis of protein location. Nat. Protoc. *1*, 729–748.

Li, J., Soroka, J., and Buchner, J. (2012). The Hsp90 chaperone machinery: conformational dynamics and regulation by co-chaperones. Biochim. Biophys. Acta *1823*, 624–635.

Li, J., Csibi, A., Yang, S., Hoffman, G.R., Li, C., Zhang, E., Yu, J.J., and Blenis, J. (2015). Synthetic lethality of combined glutaminase and Hsp90 inhibition in mTORC1-driven tumor cells. Proc. Natl. Acad. Sci. USA *112*, E21–E29.

Liao, Y., Smyth, G.K., and Shi, W. (2014). featureCounts: an efficient general purpose program for assigning sequence reads to genomic features. Bioinformatics *30*, 923–930.

Liu, W., Tanasa, B., Tyurina, O.V., Zhou, T.Y., Gassmann, R., Liu, W.T., Ohgi, K.A., Benner, C., Garcia-Bassets, I., Aggarwal, A.K., et al. (2010). PHF8 mediates histone H4 lysine 20 demethylation events involved in cell cycle progression. Nature *466*, 508–512.

Loewe, S. (1953). The problem of synergism and antagonism of combined drugs. Arzneimittelforschung *3*, 285–290.

Love, M.I., Huber, W., and Anders, S. (2014). Moderated estimation of fold change and dispersion for RNA-seq data with DESeq2. Genome Biol. *15*, 550.

Makhnevych, T., and Houry, W.A. (2012). The role of Hsp90 in protein complex assembly. Biochim. Biophys. Acta *1823*, 674–682.

Malo, N., Hanley, J.A., Cerquozzi, S., Pelletier, J., and Nadon, R. (2006). Statistical practice in high-throughput screening data analysis. Nat. Biotechnol. *24*, 167–175.

Margueron, R., Li, G., Sarma, K., Blais, A., Zavadil, J., Woodcock, C.L., Dynlacht, B.D., and Reinberg, D. (2008). Ezh1 and Ezh2 maintain repressive chromatin through different mechanisms. Mol. Cell *32*, 503–518.

Mashtalir, N., D'Avino, A.R., Michel, B.C., Luo, J., Pan, J., Otto, J.E., Zullow, H.J., McKenzie, Z.M., Kubiak, R.L., St Pierre, R., et al. (2018). Modular Organization and Assembly of SWI/SNF Family Chromatin Remodeling Complexes. Cell *175*, 1272–1288.e20.

McClellan, A.J., Xia, Y., Deutschbauer, A.M., Davis, R.W., Gerstein, M., and Frydman, J. (2007). Diverse cellular functions of the Hsp90 molecular chaperone uncovered using systems approaches. Cell *131*, 121–135.

Miao, D., Margolis, C.A., Gao, W., Voss, M.H., Li, W., Martini, D.J., Norton, C., Bossé, D., Wankowicz, S.M., Cullen, D., et al. (2018). Genomic correlates of response to immune checkpoint therapies in clear cell renal cell carcinoma. Science *359*, 801–806.

Michaud, J., Praz, V., James Faresse, N., Jnbaptiste, C.K., Tyagi, S., Schütz, F., and Herr, W. (2013). HCFC1 is a common component of active human CpG-island promoters and coincides with ZNF143, THAP11, YY1, and GABP transcription factor occupancy. Genome Res. *23*, 907–916.

Millson, S.H., Truman, A.W., King, V., Prodromou, C., Pearl, L.H., and Piper, P.W. (2005). A two-hybrid screen of the yeast proteome for Hsp90 interactors uncovers a novel Hsp90 chaperone requirement in the activity of a stress-activated mitogen-activated protein kinase, Slt2p (Mpk1p). Eukaryot. Cell *4*, 849–860.

Mosley, A.L., Sardiu, M.E., Pattenden, S.G., Workman, J.L., Florens, L., and Washburn, M.P. (2011). Highly reproducible label free quantitative proteomic analysis of RNA polymerase complexes. Mol. Cell. Proteomics *10*, M110.000687.

Moulick, K., Ahn, J.H., Zong, H., Rodina, A., Cerchietti, L., Gomes DaGama, E.M., Caldas-Lopes, E., Beebe, K., Perna, F., Hatzi, K., et al. (2011). Affinity-based proteomics reveal cancer-specific networks coordinated by Hsp90. Nat. Chem. Biol. *7*, 818–826.

O'Keeffe, B., Fong, Y., Chen, D., Zhou, S., and Zhou, Q. (2000). Requirement for a kinase-specific chaperone pathway in the production of a Cdk9/cyclin T1 heterodimer responsible for P-TEFb-mediated tat stimulation of HIV-1 transcription. J. Biol. Chem. *275*, 279–287.

Otasek, D., Morris, J.H., Bouças, J., Pico, A.R., and Demchak, B. (2019). Cytoscape Automation: empowering workflow-based network analysis. Genome Biol. *20*, 185.

Pan, D., Kobayashi, A., Jiang, P., Ferrari de Andrade, L., Tay, R.E., Luoma, A.M., Tsoucas, D., Qiu, X., Lim, K., Rao, P., et al. (2018). A major chromatin regulator determines resistance of tumor cells to T cell-mediated killing. Science *359*, 770–775.

Parker, J.B., Yin, H., Vinckevicius, A., and Chakravarti, D. (2014). Host cell factor-1 recruitment to E2F-bound and cell-cycle-control genes is mediated by THAP11 and ZNF143. Cell Rep. *9*, 967–982.

Perdew, G.H., Hord, N., Hollenback, C.E., and Welsh, M.J. (1993). Localization and characterization of the 86- and 84-kDa heat shock proteins in Hepa 1c1c7 cells. Exp. Cell Res. *209*, 350–356.

Pick, E., Kluger, Y., Giltnane, J.M., Moeder, C., Camp, R.L., Rimm, D.L., and Kluger, H.M. (2007). High HSP90 expression is associated with decreased survival in breast cancer. Cancer Res. *67*, 2932–2937.

Prince, T.L., Kijima, T., Tatokoro, M., Lee, S., Tsutsumi, S., Yim, K., Rivas, C., Alarcon, S., Schwartz, H., Khamit-Kush, K., et al. (2015). Client Proteins and Small Molecule Inhibitors Display Distinct Binding Preferences for Constitutive and Stress-Induced HSP90 Isoforms and Their Conformationally Restricted Mutants. PLoS One *10*, e0141786.

Ramírez, F., Ryan, D.P., Grüning, B., Bhardwaj, V., Kilpert, F., Richter, A.S., Heyne, S., Dündar, F., and Manke, T. (2016). deepTools2: a next generation web server for deep-sequencing data analysis. Nucleic Acids Res. *44* (*W1*), W160–W165.

Rappsilber, J., Mann, M., and Ishihama, Y. (2007). Protocol for micro-purification, enrichment, pre-fractionation and storage of peptides for proteomics using StageTips. Nat. Protoc. *2*, 1896–1906.

R Development Core Team (2008). R: A language and environment for statistical computing (R Foundation for Statistical Computing).

Richter, K., Haslbeck, M., and Buchner, J. (2010). The heat shock response: life on the verge of death. Mol. Cell *40*, 253–266.

Ritchie, M.E., Phipson, B., Wu, D., Hu, Y., Law, C.W., Shi, W., and Smyth, G.K. (2015). limma powers differential expression analyses for RNA-sequencing and microarray studies. Nucleic Acids Res. *43*, e47.

Rutherford, S.L., and Lindquist, S. (1998). Hsp90 as a capacitor for morphological evolution. Nature *396*, 336–342.

Sawarkar, R., Sievers, C., and Paro, R. (2012). Hsp90 globally targets paused RNA polymerase to regulate gene expression in response to environmental stimuli. Cell *149*, 807–818.

Scuoppo, C., Miething, C., Lindqvist, L., Reyes, J., Ruse, C., Appelmann, I., Yoon, S., Krasnitz, A., Teruya-Feldstein, J., Pappin, D., et al. (2012). A tumour suppressor network relying on the polyamine-hypusine axis. Nature *487*, 244–248.

Shannon, P., Markiel, A., Ozier, O., Baliga, N.S., Wang, J.T., Ramage, D., Amin, N., Schwikowski, B., and Ideker, T. (2003). Cytoscape: a software environment for integrated models of biomolecular interaction networks. Genome Res. *13*, 2498–2504.

Sharma, K., Vabulas, R.M., Macek, B., Pinkert, S., Cox, J., Mann, M., and Hartl, F.U. (2012). Quantitative proteomics reveals that Hsp90 inhibition preferentially targets kinases and the DNA damage response. Mol. Cell. Proteomics *11*, M111.014654.

Shi, Y., Mosser, D.D., and Morimoto, R.I. (1998). Molecular chaperones as HSF1-specific transcriptional repressors. Genes Dev. *12*, 654–666.

Sims, J.K., and Wade, P.A. (2011). SnapShot: chromatin remodeling: CHD. Cell *144*, 626–626.e1.

Su, J.M., Hsu, Y.Y., Lin, P., and Chang, H. (2016). Nuclear Accumulation of Heat-shock Protein 90 Is Associated with Poor Survival and Metastasis in Patients with Non-small Cell Lung Cancer. Anticancer Res. *36*, 2197–2203.

Taipale, M., Krykbaeva, I., Koeva, M., Kayatekin, C., Westover, K.D., Karras, G.I., and Lindquist, S. (2012). Quantitative analysis of HSP90-client interactions reveals principles of substrate recognition. Cell *150*, 987–1001.

Taipale, M., Tucker, G., Peng, J., Krykbaeva, I., Lin, Z.Y., Larsen, B., Choi, H., Berger, B., Gingras, A.C., and Lindquist, S. (2014). A quantitative chaperone interaction network reveals the architecture of cellular protein homeostasis pathways. Cell *158*, 434–448.

Tao, W., Chakraborty, S.N., Leng, X., Ma, H., and Arlinghaus, R.B. (2015). HSP90 inhibitor AUY922 induces cell death by disruption of the Bcr-Abl, Jak2 and HSP90 signaling network complex in leukemia cells. Genes Cancer *6*, 19–29.

Tariq, M., Nussbaumer, U., Chen, Y., Beisel, C., and Paro, R. (2009). Trithorax requires Hsp90 for maintenance of active chromatin at sites of gene expression. Proc. Natl. Acad. Sci. USA *106*, 1157–1162.

ten Have, S., Boulon, S., Ahmad, Y., and Lamond, A.I. (2011). Mass spectrometry-based immuno-precipitation proteomics - the user's guide. Proteomics *11*, 1153–1159.

Trapnell, C., Pachter, L., and Salzberg, S.L. (2009). TopHat: discovering splice junctions with RNA-Seq. Bioinformatics *5*, 1105–1111.

Trepel, J., Mollapour, M., Giaccone, G., and Neckers, L. (2010). Targeting the dynamic HSP90 complex in cancer. Nat. Rev. Cancer *10*, 537–549.

Tropberger, P., Pott, S., Keller, C., Kamieniarz-Gdula, K., Caron, M., Richter, F., Li, G., Mittler, G., Liu, E.T., Bühler, M., et al. (2013). Regulation of transcription through acetylation of H3K122 on the lateral surface of the histone octamer. Cell *152*, 859–872.

Tsaytler, P.A., Krijgsveld, J., Goerdayal, S.S., Rüdiger, S., and Egmond, M.R. (2009). Novel Hsp90 partners discovered using complementary proteomic approaches. Cell Stress Chaperones *14*, 629–638.

Vartholomaiou, E., Echeverría, P.C., and Picard, D. (2016). Unusual Suspects in the Twilight Zone Between the Hsp90 Interactome and Carcinogenesis. Adv. Cancer Res. *129*, 1–30.

Vasaikar, S., Huang, C., Wang, X., Petyuk, V.A., Savage, S.R., Wen, B., Dou, Y., Zhang, Y., Shi, Z., Arshad, O.A., et al. (2019). Proteogenomic Analysis of Human Colon Cancer Reveals New Therapeutic Opportunities. Cell *177*, 1035–1049.e19.

Vogel, J.L., and Kristie, T.M. (2000). The novel coactivator C1 (HCF) coordinates multiprotein enhancer formation and mediates transcription activation by GABP. EMBO J. *19*, 683–690.

Walerych, D., Kudla, G., Gutkowska, M., Wawrzynow, B., Muller, L., King, F.W., Helwak, A., Boros, J., Zylicz, A., and Zylicz, M. (2004). Hsp90 chaperones wild-type p53 tumor suppressor protein. J. Biol. Chem. *279*, 48836–48845.

Wang, R., Shao, F., Liu, Z., Zhang, J., Wang, S., Liu, J., Liu, H., Chen, H., Liu, K., Xia, M., and Wang, Y. (2013a). The Hsp90 inhibitor SNX-2112, induces apoptosis in multidrug resistant K562/ADR cells through suppression of Akt/NF-κB and disruption of mitochondria-dependent pathways. Chem. Biol. Interact. *205*, 1–10.

Wang, S., Sun, H., Ma, J., Zang, C., Wang, C., Wang, J., Tang, Q., Meyer, C.A., Zhang, Y., and Liu, X.S. (2013b). Target analysis by integration of transcriptome and ChIP-seq data with BETA. Nat. Protoc. *8*, 2502–2515.

Wang, Y., Jin, F., Wang, R., Li, F., Wu, Y., Kitazato, K., and Wang, Y. (2017). HSP90: a promising broad-spectrum antiviral drug target. Arch. Virol. *162*, 3269–3282.

Wang, Y., Wang, R., Li, F., Wang, Y., Zhang, Z., Wang, Q., Ren, Z., Jin, F., Kitazato, K., and Wang, Y. (2018). Heat-shock protein 90α is involved in maintaining the stability of VP16 and VP16-mediated transactivation of α genes from herpes simplex virus-1. Mol. Med. *24*, 65.

Whitesell, L., and Lindquist, S.L. (2005). HSP90 and the chaperoning of cancer. Nat. Rev. Cancer *5*, 761–772.

Wickham, H. (2016). ggplot2: Elegant Graphics for Data Analysis (Springer-Verlag).

Wysocka, J., and Herr, W. (2003). The herpes simplex virus VP16-induced complex: the makings of a regulatory switch. Trends Biochem. Sci. *28*, 294–304.

Wysocka, J., Myers, M.P., Laherty, C.D., Eisenman, R.N., and Herr, W. (2003). Human Sin3 deacetylase and trithorax-related Set1/Ash2 histone H3-K4 methyltransferase are tethered together selectively by the cell-proliferation factor HCF-1. Genes Dev. *17*, 896–911.

Yu, H., Mashtalir, N., Daou, S., Hammond-Martel, I., Ross, J., Sui, G., Hart, G.W., Rauscher, F.J., 3rd, Drobetsky, E., Milot, E., et al. (2010). The ubiquitin carboxyl hydrolase BAP1 forms a ternary complex with YY1 and HCF-1 and is a critical regulator of gene expression. Mol. Cell. Biol. *30*, 5071–5085.

Zargar, Z., and Tyagi, S. (2012). Role of host cell factor-1 in cell cycle regulation. Transcription *3*, 187–192.

Zhang, Y., Liu, T., Meyer, C.A., Eeckhoute, J., Johnson, D.S., Bernstein, B.E., Nusbaum, C., Myers, R.M., Brown, M., Li, W., and Liu, X.S. (2008). Model-based analysis of ChIP-Seq (MACS). Genome Biol. *9*, R137.

Zhang, H., Pandey, S., Travers, M., Sun, H., Morton, G., Madzo, J., Chung, W., Khowsathit, J., Perez-Leal, O., Barrero, C.A., et al. (2018). Targeting CDK9 Reactivates Epigenetically Silenced Genes in Cancer. Cell *175*, 1244–1258.e26.

Zhao, R., Davey, M., Hsu, Y.C., Kaplanek, P., Tong, A., Parsons, A.B., Krogan, N., Cagney, G., Mai, D., Greenblatt, J., et al. (2005). Navigating the chaperone network: an integrative map of physical and genetic interactions mediated by the hsp90 chaperone. Cell *120*, 715–727.

STAR★METHODS

KEY RESOURCES TABLE

REAGENT or RESOURCE	SOURCE	IDENTIFIER
Antibodies		
Anti-AKT1	Santa Cruz	sc-55523
Anti-GAPDH	Sigma Aldrich	G8795
Anti-H3	Abcam	ab70550
Anti-HCFC1	R & D Systems	AF6254
Anti-HCFC1	Bethyl Laboratories	A301-399A
anti-HSP90α	Abcam	ab79849
Anti-p53	Santa Cruz	sc-126
Anti-SNRNP70	Abcam	ab83306
Anti-UHRF1	Abcam	ab153972
ECL anti-mouse HRP linked	GE Healthcare	NA931V
ECL anti-rabbit HRP linked	GE Healthcare	NA934
ECL anti-rat HRP linked	GE Healthcare	NA935
Chemicals, Peptides, and Recombinant Proteins		
APC Annexin V	BD PharMingen	550474
Benzonase	Sigma Aldrich	E1014
Blasticidin S	Carl Roth	CP14.1
Bortezomib	LC Laboratories	B-1408
Chloroquine	Sigma Aldrich	C6628
DAPI	SERVA	18860.
DMEM	Sigma Aldrich	D5671
DMSO	Sigma Aldrich	41639
DRB	Santa Cruz	sc-200581
Fetal Bovine Serum	Sigma Aldrich	F7524
Foxp3 / Transcription Factor Staining Buffer Set	Thermo Fisher	00-5523-00
IMDM	Gibco	21980
Ki67-FITC	eBiosciences	8011-5699
L-Glutamine	Sigma Aldrich	G7513
Lys-C	FujiFilm Wako	129-02541
MC180295	Dr. Jean Pierre Issa, Temple University	N/A
NVP-AUY922	LC Laboratories	N-5300
Oligonucleotide Array	Agilent Biotechnologies	Custom
Penicillin Streptomycin	Sigma Aldrich	P4333
Protein A Magnetic Beads	Life Technologies	10002D
Protein G Magnetic Beads	Life Technologies	10004D
Proteinase K	Sigma Aldrich	P2308
RNase A	Applichem	A3832
RPMI 1640	Gibco	11875093
Streptavidin Dynabeads C1	Invitrogen	65001
TRI-Reagent	Sigma Aldrich	T9424
Trypsin	Promega	V5113
WST-1	Sigma Aldrich	5015944001
Zeocin	Invitrogen	R25001

(*Continued on next page*)

Continued

REAGENT or RESOURCE	SOURCE	IDENTIFIER
Critical Commercial Assays		
TurboFect	Thermo Fisher	R0532
Lipofectamine 3000	Thermo Fisher	L3000-015
Strep-Tactin Sepharose.	IBA LifeSciences	2-1201-025
PrimeScript RT Reagent Kit with gDNA Erase	Takara Bio Science	RR047
TB Green Premix Ex Taq	Takara Bio Science	RR420
NEBNext Ultra II DNA Library Prep kit for Illumina	New England Biolabs	NEB E7645S
TruSeq Stranded mRNA Library Prep Kit	Illumina	RS-122-2101
High Sensitivity DNA Chips	Agilent Technologies	5067-4626
Experimental Models: Cell Lines		
Human: Flp-In T-Rex HEK293	R. Paro, ETH Zürich	N/A
Human: HeLa	R. Paro, ETH Zürich	N/A
Human: K-562	E. Trompouki, MPI-IE Freiburg	N/A
Human: U266	Monika Engelhardt, Uniklinik Freiburg	N/A
Syrian Hamster: BHK-21 wild-type	Prof. Winship Herr and Prof. Takeharu Nishimoto	N/A
Syrian Hamster: P134S mutant cell lines	Prof. Winship Herr and Prof. Takeharu Nishimoto	N/A
Mouse: MEF cells	Thomas Jenuwein	N/A
Mouse: HPC-7	Eirini Trompouki	N/A
Deposited Data		
Sequencing Data	This paper	GSE126151
HSP90 Clients	Echeverría et al. (2011)	https://www.picard.ch/Hsp90Int/index.php
HCFC1 ChIP-seq data	ENCODE	https://www.encodeproject.org
KEGG Cell Cycle Genes	GSEA MsigDB	http://software.broadinstitute.org/gsea/msigdb/cards/KEGG_CELL_CYCLE
Protein Expression Data from COAD tumor and adjacent tissues	LinkedOmics	http://linkedomics.org/cptac-colon/
Oligonucleutides		
Refer to Table S9 for Primer Sequences	N/A	N/A
Recombinant DNA		
pC5 HSP90	This paper	N/A
pOG44	Renato Paro, ETH Zurich, Switzerland	N/A
pDEST-3FHBH-HCFC1 Kelch	This Paper	N/A
pCDNA5- HCFC1-N-terminal	Winship Herr, University of Lausanne, Switzerland	N/A
pCDNA5-HCFC1-C-terminal	Winship Herr, University of Lausanne, Switzerland	N/A
pRAB14-VP16	Christos A. Panagiotidis, University of Thessaloniki, Greece	N/A
pCP-OP_LUC	Christos A. Panagiotidis, University of Thessaloniki, Greece	N/A
pCDNA5-HCF1-fl-P134S	Winship Herr, University of Lausanne, Switzerland	N/A
pCDNA5-FL HCF1	Winship Herr, University of Lausanne, Switzerland	N/A

(*Continued on next page*)

Continued

REAGENT or RESOURCE	SOURCE	IDENTIFIER
Software and Algorithms		
MaxQuant version 1.5.2.8	N/A	https://www.maxquant.org
TrimGalore v0.4.0	N/A	http://www.bioinformatics.babraham.ac.uk/projects/trim_galore/,v0.4.0
TopHat2 v2.0.13	Trapnell et al., 2009	https://ccb.jhu.edu/software/tophat/index.shtml
Picard tools v1.1.21	N/A	http://broadinstitute.github.io/picard.
featureCounts	Liao et al., 2014	http://www.rdocumentation.org/packages/Rsubread/versions/1.22.2
DESeq2	Love et al., 2014	https://bioconductor.org/packages/release/bioc/html/DESeq2.html
vioplot	N/A	https://github.com/TomKellyGenetics/vioplot
WGCNA	Langfelder and Horvath, 2008	https://bioconductor.org/packages/release/bioc/vignettes/CVE/inst/doc/WGCNA_from_TCGA_RNaseq.html
Bowtie2	Langmead and Salzberg, 2012	https://github.com/BenLangmead/bowtie2
MACS2	Zhang et al., 2008	https://github.com/taoliu/MACS
deeptools2	Ramírez et al., 2016	https://deeptools.readthedocs.io/en/develop
pyGenomeTracks	N/A	https://github.com/deeptools/pyGenomeTracks
BioVenn	Hulsen et al., 2008	http://www.biovenn.nl
ggplot2	N/A	https://ggplot2.tidyverse.org
R Statistical Computing Software	N/A	https://www.r-project.org
gplots	N/A	https://www.rdocumentation.org/packages/gplots/versions/3.0.1.1
Homer	Heinz et al., 2010	http://homer.ucsd.edu/homer
GraphPad Prism	GraphPad Software	https://www.graphpad.com
FlowJo	FLOWJO LLC	https://www.flowjo.com/
Cytoscape	Otasek et al, 2019	https://cytoscape.org

LEAD CONTACT AND MATERIALS AVAILABILITY

Further information and requests for reagents should be directed to and will be fulfilled by the lead contact, Ritwick Sawarkar (rs2099@mrc-tox.cam.ac.uk). All unique/ stable reagents generated in this study are available from the lead contact with a completed Materials Transfer Agreement.

EXPERIMENTAL MODEL AND SUBJECT DETAILS

Flp-In T-Rex HEK293, HeLa (obtained from R. Paro, ETH Zürich), BHK-21 wild-type and the P134S mutant cell lines (kind gift from Prof. Winship Herr and Prof. Takeharu Nishimoto), and MEF cells (kind gift from Thomas Jenuwein), were cultured in DMEM supplemented with 10% Fetal Bovine Serum, 2 mM L-Glutamine, Penicillin/ Streptomycin and 5 μg/ml blasticidin. K-562 and HPC-7 cells (obtained from E. Trompouki, MPI-IE Freiburg) were grown in IMDM supplemented with 10% Fetal Bovine Serum and Penicillin-Streptomycin. U266 cells (a kind gift from Monika Engelhardt, Freiburg) were grown in RPMI supplemented with 10% Fetal Bovine Serum and Penicillin-Streptomycin. Cells were maintained at 37°C and 5% CO_2 and were routinely tested for mycoplasma contamination by PCR.

METHOD DETAILS

Chemical-Genetic Interaction Screen

The chemical genetic interaction screen was performed as described earlier (Scuoppo et al., 2012), with minor modifications. Briefly, ~2660 shRNA oligonucleotides targeting 668 different transcription regulator factors were synthesized on a 55k customized oligonucleotide array (Agilent Technologies). PCR amplified shRNAs were pool-cloned into a retroviral vector allowing doxycycline inducible expression (TREBAV; data not shown) to generate a plasmid shRNA library. The libraray was divided in 3 pools (A, B and C)

each with around 1000 shRNAs. Viruses carrying individual shRNAs were produced by transient transfection of Platinum-E retroviral packaging cells using TurboFect (Thermo Fisher #R0532) and used to infect K562 cells co-expressing the ecotropic receptor as well as the rtTA repressor. ShRNA-mediated knockdown of selected targets was achieved upon doxycycline induction (1 μg/ml doxycycline final concentration) which concurrently induced DsRed expression. Cells were simultaneously treated with either DMSO (mock treatment) or with 15 nM NVP-AUY922 (Hsp90 inhibitor, LC Laboratories, USA). Four days upon treatment cells were harvested and barcodes were deep-sequenced. The experiment was performed in two biological replicates for each pool of shRNA (A1, A2, B1, B2, C1 and C2). Thus we have 5 sets of samples (Day0, Day4untreated, day4dox, day4NVP, day4doxNVP) processed in 6 subpools (A1, A2, B1, B2, C1 and C2) making up a total of 30 samples. To determine the Chemical-Genetic Interaction Score (CGIS), the following two steps were performed: (1) the quotient between the shRNA counts of HSP90-inhibitor treated and untreated samples, both after shRNA induction by doxycycline, was calculated to determine the fold change for each shRNA. (2) the log-2 based fold change values for all shRNAs targeting the same gene added to calculate the CGIS. Five different cut-offs for CGIS were used to filter the list of all genes tested. Analysis of the different list showed robustness of our findings to different cut-offs used (Figure S4C). Finally, a CGIS cut-off of ± 1.5 was used which is equivalent to the standard deviation of ~1. Test of association between CGIS-shortlist and known HSP90 clients was done using chi-square test. A list of known HSP90 clients was downloaded from https://www.picard.ch/Hsp90Int/index.php as of January 2019.

Since the CGIS outlined above does not consider the variation between duplicate experiments as well as for individual shRNA, we also performed a Z-score based analysis as described in the reference (Malo et al., 2006). The CGIS of a gene is a cumulative score for all shRNA targeting that gene (shown in Figure 1C) whereas the Z-score is calculated for individual shRNAs (shown in Figure 1D). The average standard deviation for all shRNAs targeting the same gene across the whole population was ~0.07, indicating highly reproducible effects between the different shRNAs.

Cell Fractionation

Fractionation was performed as described earlier (Margueron et al., 2008). Briefly, HEK cells were harvested and an aliquot was taken out in RIPA buffer (50 mM HEPES pH 7.9, 150 mM NaCl, 0.5% sodium deoxycholate, 0.1% SDS, 1% Triton-X, 5 mM $MgCl_2$, 10% glycerol), and saved as cell extract. Remaining cells were resuspended in Buffer A (10 mM HEPES pH 7.9, 5mM $MgCl_2$, 0.25 M Sucrose) and incubated on ice for 10 minutes. NP-40 detergent was added to the cell suspension to a final concentration of 0.1% for HEK. Cells were then passed through an 18G needle (10 times for HEK) and centrifuged at 2000 xg for 10 min at 4°C. The resulting supernatant was saved as cytosol. The nuclear pellet was washed twice with buffer A. An aliquot was taken out in RIPA buffer and saved as total nuclear extract (TNE). The rest was resuspended in 0.5M buffer B (20 mM HEPES pH 7.9, 0.5 M KCl, 1.5 mM $MgCl_2$, 0.1 mM EDTA, 10% Glycerol) and incubated for 30 min at 4°C. The suspension was centrifuged and supernatant was saved as nucleoplasm. The chromatin pellet was resuspended in 2M buffer B (20 mM HEPES pH 7.9, 2 M KCl, 1.5 mM $MgCl_2$, 0.1 mM EDTA, 10% Glycerol), and incubated for 30 min at 4°C. TCE, TNE and chromatin (CHR) were sonicated for 15 cycles (30 s on/30 s off, high power) using Bioruptor sonicator. Samples were centrifuged at 20 000 xg for 10 min to remove debris and protein amount was determined by Nanodrop.

SDS-PAGE

Polyacrylamide gels were cast according to Rotiphorese® Gel 30 (ROTH, #30291) instruction manual. Protein samples were mixed with 4X loading buffer (50 mM Tris-HCl pH 6.8, 2% SDS, 10% glycerol, 1% β-mercaptoethanol, 0.02% bromophenol blue), heated at 95°C for 5 min and loaded on gels. Electophoresis was then run at 150-180 V for 60-90 min in SDS-PAGE running buffer (25 mM Tris, 192 mM glycine, 0.1% SDS).

Silver Staining

Polyacrylamide gels were fixed in fixation solution (10% HOAc, 45% MeOH) for 15 min and reduced in Farmer's reducer solution (30 mM $K_3Fe(CN)_6$, 30 mM $Na_2S_2O_3$) for 2 min. Upon several extensive washes gels were stained in 0.1% (g/v) silver nitrate, washed again, and developed with 0.1% formaldehyde in 2.5% Na_2CO_3. Reaction was stopped by addition of 10% HOAc.

Western Blotting

Transfer of proteins on nitrocellulose membrane was carried out at 300 mA for 60 min in transfer buffer (25 mM Tris, 192 mM glycine, 20% methanol). Membrane was then blocked with blocking solution (5% non-fat milk in PBST), incubated with primary (for 1 hour or ON) and secondary antibody (for 1 hour) and developed using ChemiDoc Imaging System (Biorad).

Nuclear Protein Affinity Purification Coupled to Mass Spectrometry

Stable Cell Lines Generation

Hsp90α cDNAs was cloned into pC5 destination vector. Flp-In HEK293 T-REx cells stably expressing the tet repressor were co-transfected with the corresponding expression plasmids and the pOG44 vector (for co-expression of the Flp-recombinase) using the Lipofectamine 3000 (Life Technologies, #L3000-015) according to manufacturer's protocol. Cells were selected in zeocin-containing medium (100 μg/ml) for 2–3 weeks to generate stable cell lines. Resulting HA-Strep tagged protein clones were used for further experiments.

Nuclear Protein Extract Preparation

Flp-In HEK293 T-REx cells stably expressing Hsp90α or RFP were grown to 70% confluency. Recombinant protein expression was induced by adding 1 μg/ml tetracyclin directly into growing medium for 16 hours. Cells were collected and nuclei were then isolated as already described earlier. Nuclear protein extracts were generated using the classical high-salt Dignam extraction protocol (Dignam et al., 1983) with slight modifications. Briefly, nuclei were resuspended in buffer B (20 mM HEPES pH 7.9, 420 mM KCl, 1.5 mM $MgCl_2$, 0.1 mM EDTA, 10% glycerol) and incubate for 30 min at 4°C. Suspension was diluted in buffer D (20 mM HEPES pH 7.9, 1.5 mM $MgCl_2$, 10% glycerol), treated with benzonase (10 U/ml), and centrifuged at 70 000 xg for 30 min at 4°C. Supernatant was recovered and immediately used for protein affinity purification.

Buffers A, B and D contained ATP regeneration system components (10 mM ATP, 0.2 M phosphocreatine, 1 mg/ml creatine kinase) to keep ATP concentration high enough for the ATP-dependent cycle of the chaperone.

Protein Affinity Purification

Affinity purification of recombinant HA-Strep-tagged proteins was performed utilizing the IBA GmbH *Strep*-tag® - *Strep*-Tactin system (IBA, #2-1201-025). Briefly, sample was applied to the column to pass through gravity force. Following six washes with washing buffer (20 mM HEPES pH 7.9, 1.5 mM $MgCl_2$, 10% Glycerol, 150 mM KCL, 0.1% NP-40) bound complexes were released with elution buffer (20 mM HEPES washing buffer. pH 7.9, 1.5 mM $MgCl_2$, 10% glycerol, 150 mM NaCl, 20 mM desthiobiotin, 0.1% NP-40). Eluates were snap frozen in liquid nitrogen and kept at – 80°C until needed.

Protein Digestion and Mass Spectrometry Analysis

Combined elution fractions of the Streptactin Sepharose purified protein complexes were TCA precipitated, washed with −20°C neat acetone, air-dried and finally resuspended in 50 μl urea buffer (10 mM HEPES-NaOH, pH 7.9, 6 M urea, 2M thiourea) and the pH was adjusted to pH 7-8 by addition of 1M Tris-HCl, pH 10. Reduction/alkylation was carried out by adding TCEP to a final concentration of 5 mM (20 min, 25°C) followed by iodoacetamide to a final concentration of 10 mM (15 min, 25°C). Samples were first subjected to Lys-C (Wako; 250 ng, 25°C, 3 hr) proteolysis and after addition of 0.2 mL 50 mM ammonium bicarbonate subsequently digested with Promega trypsin (250 ng, 25°C, 12 hr) and analyzed by nanoLC-MS as previously published (Tropberger et al., 2013) with modifications outlined below. STAGE tip assisted sample purification of digested samples was achieved essentially as described (Rappsilber et al., 2007). Desalted samples were subsequently analyzed using nanoflow (Agilent 1200 nanoLC, Germany) LC-MS/MS (precisely as reported in Engelke et al., 2014) on a linear ion trap (LIT)-Orbitrap (LTQ-Orbitrap XL+ETD) mass spectrometer (Thermo Fisher Sci., Germany). Peptides were eluted with a linear gradient of 10%−60% buffer B (80% ACN and 0.5% acetic acid) at a flow rate of 250 nl/min over 90 min. Each sample was analyzed twice, employing CID (collision induced dissociation) or ETD (electron transfer dissociation) fragmentation for the generation of MS^2 spectra. Data were acquired using a DDA "top 5" method, dynamically choosing the five most abundant precursor ions from the survey scan (mass range 350−1600 Th) in order to isolate and fragment them in the LIT. All data were acquired in the profile mode and dynamic exclusion was defined by a list size of 500 features and exclusion duration of 30 s with a MMD of 10 ppm. Early expiration was disabled to decrease the re-sequencing of isotope clusters. The isolation window for the precursor ion selection was set to 2.0 Th (CID) and 2.5 Th (ETD), respectively. Precursor ion charge state screening was enabled and all unassigned charge states as well as singularly charged ions were rejected. For the survey scan a target value of 1,000,000 (1000 ms maximal injection time) and a resolution of 60,000 at *m/z* 400 were set (with lock mass option enabled for the 445.120024 ion), whereas the target value for the fragment ion spectra was limited to 10,000 ions (200 ms maximal injection time). The general mass spectrometric conditions were: spray voltage, 2.3 kV; no sheath and auxiliary gas flow; ion transfer tube temperature, 160°C; collision gas pressure, 1.3 mTorr. Ion selection thresholds for MS^2 were 1000 counts (for both CID and ETD). For CID the normalized collision energy (NCE) using wide-band activation mode was set to 35% and an activation q = 0.25 and activation time of 30 ms was applied. We enabled supplementary activation (NCE 15%) for ETD, the default charge state was set to 3 and a fluoranthene anion activation time of 100 ms was used. General ETD reagent ion source parameters were set as follows: polarity, negative; temperature, 160°C; emission current, 50 μA; electron energy, −70V; CI pressure, 25 psi; reagent vial 1 target value, 300,000 and temperature, 90°C.

MS data were processed by MaxQuant (version 1.5.2.8) and searched with the integrated Andromeda database search engine against the human Uniprot database (release October 2014) combined with frequently observed contaminants and concatenated with the reversed versions (decoys) of all sequences. In addition the N-terminal HA-twin_StrepII double tag (MYPYDVPDYAG TELGSTMASWSHPQFEKGGGSGGGSGGGSWSHPQFEKAAD) was appended as a separate protein sequence to the database. The MMD for monoisotopic precursor ions and MS/MS peaks were restricted to 7 ppm and 0.6 Da, respectively. Enzyme specificity was set to trypsin (permitting a maximum of two missed cleavages) allowing cleavage N-terminal to proline and between aspartate and proline. Modifications were cysteine carbamidomethylation (fixed) as well as protein N-terminal acetylation, deamidation (asparagine and glutamine) and methionine oxidation as variable PTMs. The required peptide false discovery rate (FDR) and the required protein FDR were set to 0.01, with the minimum required peptide length of 6 amino acids. The "match between runs" and "second peptide" features were enabled. Proteins were identified with at least two peptides, wherein one of them should be unique to this protein. Intensity-based relative and absolute quantifications were performed using MaxLFQ, the label-free quantification (LFQ) and iBAQ algorithms implemented in MaxQuant (Deeb et al., 2014). Protein quantification ratios were calculated only for proteins with $\geq$ 2 LFQ measurements, requiring at least one MS^2 measurement to be associated with the MaxLFQ quantified peptide ion isotope cluster peak (feature) in order to be considered as valid. The LFQ values calculated for the two tryptic peptides derived from the HA-twin_StrepII double tag were utilized for additional normalization of samples in order to account for variations in the

amount of bait proteins (HSP90α and RFP control). Nuclear HSP90α interactome analysis was performed in 4 biological replicates using RFP-expressing HEK cells as a control. A ratio between peptide intensity in HSP90 and RFP pull-downs for individual protein hits was calculated. Proteins with the peptide-intensity ratio of more than 4 were identified as HSP90α-interacting candidates per replicate. Candidate proteins identified in at least 3 out of 4 replicates were considered as HSP90α physical interactors (Table S3). Manual curation for transcription regulators from this list gave rise to Table S4 that has been used for all further analyses in this study. Four different cut-offs for log2 fold enrichment was used to analyze the robustness of our findings (Figure S4D).

Network visualization of genetic and physical interactors was done using Cytoscape with default parameters (Shannon et al., 2003) with information of protein-protein interactions known in literature. For the sake of available space in the figure and clarity, not all genes are shown. Both networks (Figures 1E and 2E) show only those genes which either have more than one known interaction with other genes in the list or are known parts of a complex, other subunits of which were in the list.

Manual curation of HCFC1 interactors was done by combining interactors found in diverse cell lines in different labs in the last few years, the source references of these data are indicated in the main text. These HCFC1 interactome data were used in Figures 3E, 4C, and S4F. Annotation of subunits of NuRD and BAF complexes (Figure 3E) is based on references (Bao and Shen, 2007; Kasten et al., 2011; Mashtalir et al., 2018; Sims and Wade, 2011).

RNA Isolation

RNA isolation was done using TRI-Reagent (Sigma Aldrich, #T9424) according to manufacturer's instructions. For HEK293 and HeLa, cell lysis was done directly on the cell culture dish. 1ml of TRI-Reagent was used per 10 cm. For K562, cells were pelleted by centrifugation and resuspended in 1ml of TRI-Reagent per $10x10^6$ cells. Samples were incubated at room temperature for 5 min to dissociate nucleo-protein complexes. 0.2 mL of chloroform was added per 1ml of TRI-Reagent used for cell lysis. Samples were shaken vigorously 15 s, incubated at room temperature for 10 min and spun down at 12 000 x g for 10 min at 4°C. The upper aqueous phase was transferred into a fresh tube and supplemented with isopropanol (0.5 mL per 1 mL of TRI-Reagent used). Sample was mixed by inverting and incubated at room temperature for 5-10 min. RNA pellet was washed with 1 mL of 75% ethanol by centrifuging at 10000 g for 10 min at 4°C. It was air-dried and re-dissolved in water. RNA concentration was measured using Nanodrop 1000.

ChIP-Seq

Preparation of chromatin

Twenty million K562, treated with DMSO or 300nM NVP-AUY922 for 16 hours were fixed using 1% methanol-free formaldehyde in IMDM for 10 min at room temperature (end-over-end rotation). The cross-linking reaction was stopped by adding glycine to a final concentration of 125 mM and incubated for 5 min at room temperature (end-over-end rotation). Cells were spun down at 750 xg for 5 min at 4°C and washed twice with cold PBS. Chromatin preparation for K652 was performed according to Arrigoni et al. (2016). Briefly, cell pellet sonicated in Farnham Buffer (5 mM PIPES pH 8, 85 mM KCl, 0.5% Igepal) with Covaris sonicator to isolate nuclei. The following settings were used: Peak Power = 75, Duty Factor = 2, Cycles/Burst = 200, Time = 2. Nuclei were then washed in Farnham buffer and resuspended in shearing buffer (10 mM Tris-HCl pH 8, 0.1% SDS, 1 mM EDTA). Material was sonicated in 1 mL Covaris tubes using the following settings: Peak Power = 140, Duty Factor = 5, Cycles/Burst = 200, Time = 25-30 min. Obtained chromatin was spun down at 20 000 xg for 10 min at 4°C to remove debris. A small aliquot of sheared chromatin was processed in order to assess sonication efficiency and chromatin yield prior to IP - the optimal size range of DNA for ChIP-seq analysis should be between 200 and 600 base pairs. Prior to IP chromatin was diluted 1:1 with lysis buffer 3 to achieve a final SDS concentration of 0.05%. An aliquot was saved as input DNA.

Chromatin Immunoprecipitation

Chromatin Immunoprecipitation was performed as previously described (Lee et al., 2006). Briefly, Protein A or G magnetic beads were incubated with 5ug of antibody in block solution for 6 hours at 4°C. Bead-antibody complex was then incubated with 200ug of chromatin overnight at 4°C solution. Beads were washed once with wash buffer 1 (20 mM Tris-HCl pH 8, 150 mM NaCl, 2mM EDTA, 0.1% SDS, 1%Triton X-100), wash buffer 2 (20 mM Tris-HCl pH 8, 500 mM NaCl, 2 mM EDTA, 0.1% SDS, 1%Triton X-100) and wash buffer 3 (10 mM Tris-HCl pH 8, 250 nM LiCl, 2 mM EDTA, 1% NP40) and TE. DNA was eluted by addition of 200 μL elution buffer (50 mM Tris-HCl, pH 8.0, 10 mM EDTA and 0.5% – 1% SDS) to beads and heating at 65°C for 45 min under vigorous shaking. Upon reverse crosslinking DNA was treated with RNase and proteinase K, and was purified by Phenol–chloroform–isoamyl alcohol extraction.

Library Prep

For ChIP-seq, DNA libraries were prepared from the immunoprecipitated DNA. Sequencing libraries were prepared using the NEBNext Ultra II DNA Library Prep kit for Illumina (NEB E7645S). 2-5 ng of immunoprecipitated DNA was used for library preparation. Library size distribution was monitored by capillary electrophoresis (Agilent 2100 Bioanalyzer, High Sensitivity DNA Chips (Agilent, 5067–4626). Libraries were sequenced paired-end on HiSeq 3000. Sequencing Depth was 9M for ChIP and 95M for Input, paired end for length of 75bps.

Biochemical Analyses of Protein Stability and Interactions

FLAG- and biotin-tagged HCFC1 Kelch domain (this paper) or HCFC1 N-/ C-terminal fragments (kind gift from Prof. Winship Herr, Lausanne, Switzerland) were expressed in HEK293 or HeLa cells as indicated in respective figures. To strengthen the transient

interaction between Hsp90 and HCFC1 cells were co-transfected with a mutant of HSP90 (E42A; deficient in ATP hydrolysis; Prince et al., 2015) which binds but does not release its clients. Total cell extracts were prepared as described by Moulick et al. (2011). Biotin-tagged bait proteins were purified using streptavidin magnetic Dynabeads.

To determine the role of autophagy and proteasome in degrading HCFC1 upon HSP90 inhibition, HEK293 cells were treated with the following inhibitors indicated in Figure S7A: 300nM NVP-AUY922; 50nM Bortezomib; 15uM Chloroquine.

Experiments Testing Functional Interaction between HSP90 and HCFC1

Effect of HCFC1 knockdown on mean growth rate of K562 cells was measured in the presence and absence of HSP90in (Figure 6A). K562 cells were infected with the indicated shRNAs linked to GFP and either treated with 15nM HSP90 inhibitor or left untreated. Effect of HCFC1 knockdown on cell growth was assessed by flow cytometric measurement of the fraction of GFP^+ cells, reflecting growth rate of $shRNA^+$ GFP^+ cells relative to $shRNA^-$ GFP^- cells in the same population. The graph shows the relative change in the fraction of GFP^+ cells 7 days after infection. A general increase in the fraction of GFP^+ cells is seen as it takes a few days for all infected cells to express sufficient GFP to be detected by FACS. At 15nM concentration of HSP90in, wild-type cells typically show very little effect on growth rate.

To study if HCFC1 overexpression can rescue effects of HSP90in on cell-cycle gene expression (Figure S7D), we transfected HeLa cells with HCFC1-expression constructs (kind gift from Prof. Winship Herr, University of Lausanne, Switzerland). 2 days after transfection, 300nM HSP90in was added for 6 hours before lysing the cells in Trizol for expression analyses.

HSP90 Inhibitor Sensitivity of BHK Isogenic Cells

Two cell lines, BHK-21 wild-type and the P134S mutant cell lines (kind gift from Prof. Winship Herr, University of Lausanne, Switzerland and Prof. Takeharu Nishimoto, Japan), were seeded at a density of 10,000 cells per well in 96-well plates and treated with 15nM of the Hsp90 inhibitor, NVP-AUY922. The cells were incubated at 39.5°C and cell viability was measured 48 hours after seeding using WST-1 reagent from Sigma. The interaction between HSP90 and HCFC1 was tested in BHK isogenic cells by transfecting biotin-tagged HSP90 and performing affinity purifications following protocol detailed above.

HSP90/CDK9 Inhibitor Combination Treatment of Various Cell Lines

Cell lines were incubated with the following inhibitor concentration at indicated cell numbers. Cell viability was measured 24 or 48 hours after seeding using WST-1 reagent from Sigma, as shown in the table below.

Cell Line	Seeded Cells Per well (96 well plate)	CDK9 Inhibitor[#]	Conc.	HSP90 Inhibitor	Conc.	Time
U266	10k	DRB	50 uM	AUY922	12.5nM	48h
U266	20k	MC180295	150nM	AUY922	15nM	24h
K562	20k	DRB	50 uM	AUY922	15nM	24h
K562	20k	MC180295	1uM	AUY922	15nM	24h
HeLa	20k	MC180295	1uM	AUY922	50nM	24h
BHK21 (isogenic wild-type and mutant)	10k	-	-	AUY922	15nM	48h

[#]MC180295 was a kind gift from Dr Jean-Pierre Issa (Temple University, USA).

Viral Transcription Reporter Assay

HEK293 cells were plated in a 24-well plate 24hrs prior to transfection. Cells were co-transfected with Herpes Simplex Virus-alpha promoter driven-Luc reporter plasmid (pCP-OP_LUC; 0.5ug) and trans-activator VP16 plasmid (pRAB14-VP16) at a 1:0.3 molar ratio (Bohenzky et al., 1993). The plasmids were a kind gift from Christos A. Panagiotidis from Aristotle University of Thessaloniki, Greece. Luciferase expression was measured 24hrs post-transfection and normalized to GAPDH endogenous control by RT-qPCR. HSP90in was added at 10nM concentration 6hrs prior to harvesting cells. P134S mutant HCFC1 was expressed from pCDNA5-HCF1-fl-P134S plasmid, and wild-type HCFC1 from pCDNA5-FL HCF1, both obtained as a kind gift from Prof. Winship Herr, University of Lausanne, Switzerland.

Apoptosis and Cell-Cycle Analyses of U266 Cells Treated with Inhibitors (Figure S9B)

Cells were washed twice by centrifugation in phosphate-buffered saline (PBS) at 500 g for 5 min. Fixation, permeabilization and staining were performed using Foxp3/Transcription factor Staining buffer set (eBioscience) according to manufacturer's instructions with minor modifications. Cells were stained at 4°C in the dark. The annexin V/ DAPI staining was used to determine apoptosis according to manufacturer's protocol with minor modifications (BD pharmingen). Staining with Annexin V (1:50 dilution) conjugated to APC and DAPI (2ug/ml) was performed in annexin V binding buffer at a concentration of 0.5-1.0 × 10^7 cells/ml. Flow cytometry was performed using the BD LSR II flow cytometer on 10,000 events and analyzed using FlowJo software. For cell-cycle analysis, Ki67-FITC

(eBioscience) was used at a 1:500 dilution and DAPI at 2ug/ml. Cells were then washed, resuspended in PBS and analyzed using the BD LSR II flow cytometer on 10,000 events. Data were analyzed using FlowJo software.

Quantitative PCR

RNA was isolated after Trizol extraction per manufacturer's protocol. RT was done using PrimeScript RT with dDNA eraser (Takara) and cDNA amplified using TB GReen Premix Ex Taq (Takara) per manufacturers instructions. DNA amounts were quantified using the ΔΔCT, and the non treated condition was set to one.

RNA-Seq

HSP90 inhibition was carried out using the following concentrations of NVP-AUY922 for 16 hours with the corresponding cell types: 50nM for HPC-7, 200nM for MEFs and 300nM for K562. RNA was isolated using Trizol as described above. Library Preparation was done using TruSeq Stranded mRNA, according to manufactures protocol. Samples were sequenced using. Samples were sequenced using Illumina NextSeq 500 for MEF and K562 cells and Illumina NextSeq 2500 for HPC-7 cells, paired end and read length of 75bps. Sequencing Depth was 9M and 15M for HPC-7 cells, 10M and 15M for K562, and 13M for MEF cells. Samples were sequenced using Illumina NextSeq 500 for MEF and K562 cells and Illumina NextSeq 2500 for HPC-7 cells.

QUANTIFICATION AND STATISTICAL ANALYSIS

Computational Analysis of Sequencing Data

RNA-seq reads were trimmed with TrimGalore (http://www.bioinformatics.babraham.ac.uk/projects/trim_galore/, v0.4.0) and mapped to Gencode (GRCh37, release: 19 or GRCm38, release m4, respectively) annotation using TopHat2 (Kim et al., 2013) (v2.0.13) with the options mate-inner-dist, mate-std-dev and library-type (fr- firststrand). The distance between read mates (mate-inner-dist and mate-std-dev) were assessed individually using Picard tools [http://broadinstitute.github.io/picard.] (v1.1.21). After mapping of the RNA-seq reads from all samples, the reads that mapped uniquely to the genome were counted using featureCounts (Liao et al., 2014) with the following options: -Q 10 -p -B -C -s 2. The annotations present in the *Homo sapiens* gtf file from the Ensembl release 75 were used as reference for counting. DESeq2 (Love et al., 2014) was used for differential expression analysis of all replicates for each condition. Genes with an adjusted p value < 0.01 and absolute log2 fold change more than 1 were defined as significantly affected.

A list of KEGG cell cycle genes were downloaded from GSEA MSigDB (http://software.broadinstitute.org/gsea/msigdb/cards/KEGG_CELL_CYCLE). Genes were grouped into HCFC1 target and non-target genes based on the presence or absence, respectively, of HCFC1 ChIP-seq peak in their promoter region (ENCODE data). Violin plots in Figure S7B showing log2 fold changes in expression upon HSP90 inhibition was plotted for both groups using the vioplot package in R (https://github.com/TomKellyGenetics/vioplot). Significance was calculated using a Wilcoxon test.

Raw read counts from TCGA RNA-seq data were downloaded using TCGAbiolinks R package (Colaprico et al., 2016). Raw counts were first transformed to normalized log2-counts per million (logCPM) using the voom method within limma (Ritchie et al., 2015) and then centered gene-wise for between-sample comparisons. Only cancer types with more than 5 normal tissue controls were used for further analysis (17 cancer types remained after filtering). Heatmaps were generated using the "gplots" R package (https://www.rdocumentation.org/packages/gplots/versions/3.0.1.1) using the following score ($median_{PT}$-$median_{NT}$)/($median_{PT}$+$median_{NT}$). Hierarchical clustering with euclidean distance metric and ward method was performed using the heatmap.2 function available in the "gplots." The resulting hierarchical tree was split into 25 clusters. Four additional number of clusters (15, 20, 30 and 35) were used to demonstrate that the results of our analysis are not dependent on the cut-offs used (Figure S4E).

WGCNA (Langfelder and Horvath, 2008) analysis was used to identify modules of genes that are co-expressed in all cancer types analyzed in this study including normal tissue and primary tumor samples. Analysis was performed according a WGCNA tutorial (https://bioconductor.org/packages/devel/bioc/vignettes/CVE/inst/doc/WGCNA_from_TCGA_RNAseq.html).

TCGA cancer type acronyms: BLCA (bladder urothelial carcinoma), BRCA (breast invasive carcinoma), COAD (Colon adenocarcinoma), CHOL (cholangiocarcinoma), ESCA (esophageal carcinoma), HNSC (head and neck squamous cell carcinoma), KICH (kidney chromophobe), KIRC (kidney renal clear cell carcinoma), KIRP (kidney renal papillary cell carcinoma), LIHC (liver hepatocellular carcinoma), LUAD (lung adenocarcinoma), LUSC (lung squamous cell carcinoma), PRAD (prostate adenocarcinoma), READ (Rectum adenocarcinoma), STAD (stomach adenocarcinoma), THCA (thyroid carcinoma), UCEC (uterine corpus endometrial carcinoma).

ChIP-seq reads were aligned to the human genome build hg38 or mouse genome mm10, respectively, using Bowtie2 (Langmead and Salzberg, 2012). Duplicate and discordant reads were removed. Peak calling was done with MACS2 (model- based analysis of ChIP- Seq) (Zhang et al., 2008) using "–keep-dup all," "–nomodel" and "–extsize 200." Gene annotations and transcript start site (TSS) information for human genes were from taken from Gencode annotation release 26 and for mouse genome from Gencode annotation release m4. For visualization, the paired-end reads were extended to fragment size and normalized to total reads aligned (reads per million, RPM) using deeptools2 (Ramírez et al., 2016). Profile plots and heatmaps of ChIP-seq signal were generated with deeptools2 (Ramírez et al., 2016).

All browser tracks were visualized using pyGenomeTracks program (https://github.com/deeptools/pyGenomeTracks). Venn diagram was visualized using BioVenn (Hulsen et al., 2008).

BETA package (Wang et al., 2013b) was used to predict the activating/repressive function of HCFC1 on its target genes in mouse embryonic stem cells.

Publicly available ChIP-seq data for HCFC1, ZNF143, THAP11, GAPB and YY1 in HeLa cells were downloaded from GEO accession GSE31419. ChIP-seq data for E2F1, E2F4 and E2F6 in HeLa cells as well as HCFC1 in mouse ESCs were downloaded from ENCODE.

Gene Set Analysis (GSA)

Gene Set Analysis was first described in Efron and Tibshirani (2007). GSA for genes interacting with HSP90 or HCFC1 was done as described in Hadizadeh Esfahani et al. (2018). In our analysis, GSA method calculates a score for each gene based on its expression in cancer tissues compared to control tissues using the t-statistic. The GSA analysis further combines these scores of individual genes within a set to a singular value termed as ''delta GSA value of the gene set'' using the max-mean statistic. GSA values for different gene sets were plotted as scatterplots using ggplot2 (Wickham, 2016). Correlation and F-Statistics were calculated using the lm() function from the stats package (R Core Development Team, 2018). Heatmaps were plotted using ''gplots.'' TCGA cancer type acronyms are indicated above.

Protein Expression Visualization

Protein expression data from COAD tumor and normal adjacent tissues (Vasaikar et al., 2019) was downloaded from LinkedOmics (http://linkedomics.org/cptac-colon/). Boxplots were plotted using ''ggplot2.''

Motif Discovery

Motif discovery was done for promoter regions of genes misregulated upon HSP90 inhibition as well as for HSP90 ChIP-seq peak regions using Homer software (Heinz et al., 2010) with default parameters except '–size given' for peak regions. For misregulated genes, the promoter region was defined as 400bp upstream of the transcription start site (TSS) to 100bp downstream of the TSS following a Homer tutorial ((http://homer.ucsd.edu/homer/microarray/index.html). Genes upregulated and downregulated upon HSP90 inhibition were used separately for the motif analysis.

Statistical Tests

Statistical tests used to plot each figure are indicated in their respective legends.

DATA AND CODE AVAILABILITY

All the deep-sequencing data in this study are deposited in GEO and are available under accession number GEO: GSE126151